The development of the eastern Orpheus rift basin, offshore eastern Canada: A case study of the interplay between rift-related faulting and salt deposition and flow

Bari R. Hanafi[1*], Martha O. Withjack[1], Michael A. Durcanin[1,2], Roy W. Schlische[1]

[1]Department of Earth and Planetary Sciences, Rutgers University, Piscataway, New Jersey, 08854, USA

[2]Murphy Exploration and Production Company, Houston, Texas 77024, USA

*Corresponding author email: brhanafi@eps.rutgers.edu

ABSTRACT

The salt-rich Orpheus rift basin, part of the eastern North American (ENAM) rift system, formed during the Late Triassic to Early Jurassic prior to opening of the Atlantic Ocean. Using a dense grid of 2D seismic-reflection lines, data from nearby wells, and information from adjacent ENAM rift basins, we have established a tectonostratigraphic framework, identified key structural elements, and reconstructed the deformation history for the eastern part of the basin. Our work shows that a series of E-striking, S-dipping faults with normal separation bound the basin on the north. Deformation within the basin is complex with fault-propagation folds above deep-seated, intrabasin faults, detachment folds, detached thrust faults, and salt diapirs. The synrift salt consists of a lower massive unit that underlies a younger unit with two distinct interfingering facies. Facies A, consisting of salt and interbedded sedimentary rocks (likely shales), developed near the border-fault system and its relay ramps. Facies B, consisting of massive salt with few interbedded sedimentary rocks, developed within the basin center. The youngest synrift unit accumulated exclusively within minibasins near the northern border-fault system. Based on location, this unit likely consists of coarse-grained and poorly sorted alluvial-fan or talus-slope deposits shed from the footwall. All synrift units are intruded by igneous sheets

likely associated with the Central Atlantic Magmatic Province and, thus, are mostly Late Triassic (or possibly older). The border-fault system profoundly affected deposition within the eastern Orpheus rift basin by providing pathways for clastic sediment input into the salt-rich basin. These depositional patterns subsequently influenced deformation associated with lateral salt flow during minibasin formation. In regions with interbedded salt, detachment folds and thrust faults developed, whereas salt walls and columns developed in regions with more massive salt.

1. INTRODUCTION

The eastern North American (ENAM) rift system that formed during the breakup of Pangea extends from the southeastern United States to southeastern Canada. It has three geographic segments with distinct tectonic histories (Fig. 1a). Rifting was underway in all segments by Late Triassic time, but rifting ceased diachronously, first in the southern segment (latest Triassic/earliest Jurassic), then in the central segment (Early Jurassic), and finally in the northern segment (Early Cretaceous) (Withjack et al., 1998; Withjack and Schlische, 2005; Withjack et al., 2012).

Outcrop data (together with limited borehole and seismic-reflection data) from the exposed onshore rift basins have supplied important information about the stratigraphy, structure, and tectonic history of the ENAM rift system (e.g., Olsen et al., 1996; 2003; Schlische et al., 2003; Withjack et al., 2009; Withjack et al., 2013). Critical questions, however, remain about the subsurface geology and timing of deformation for the ENAM rift system. The availability of high-quality, industry, borehole and seismic-reflection data from several of the offshore ENAM

rift basins provide the opportunity to address these questions by better defining the subsurface

stratigraphy and structure of the ENAM rift system and constraining the timing of deformation

and, thus, the tectonic history of the ENAM margin during and after rifting.
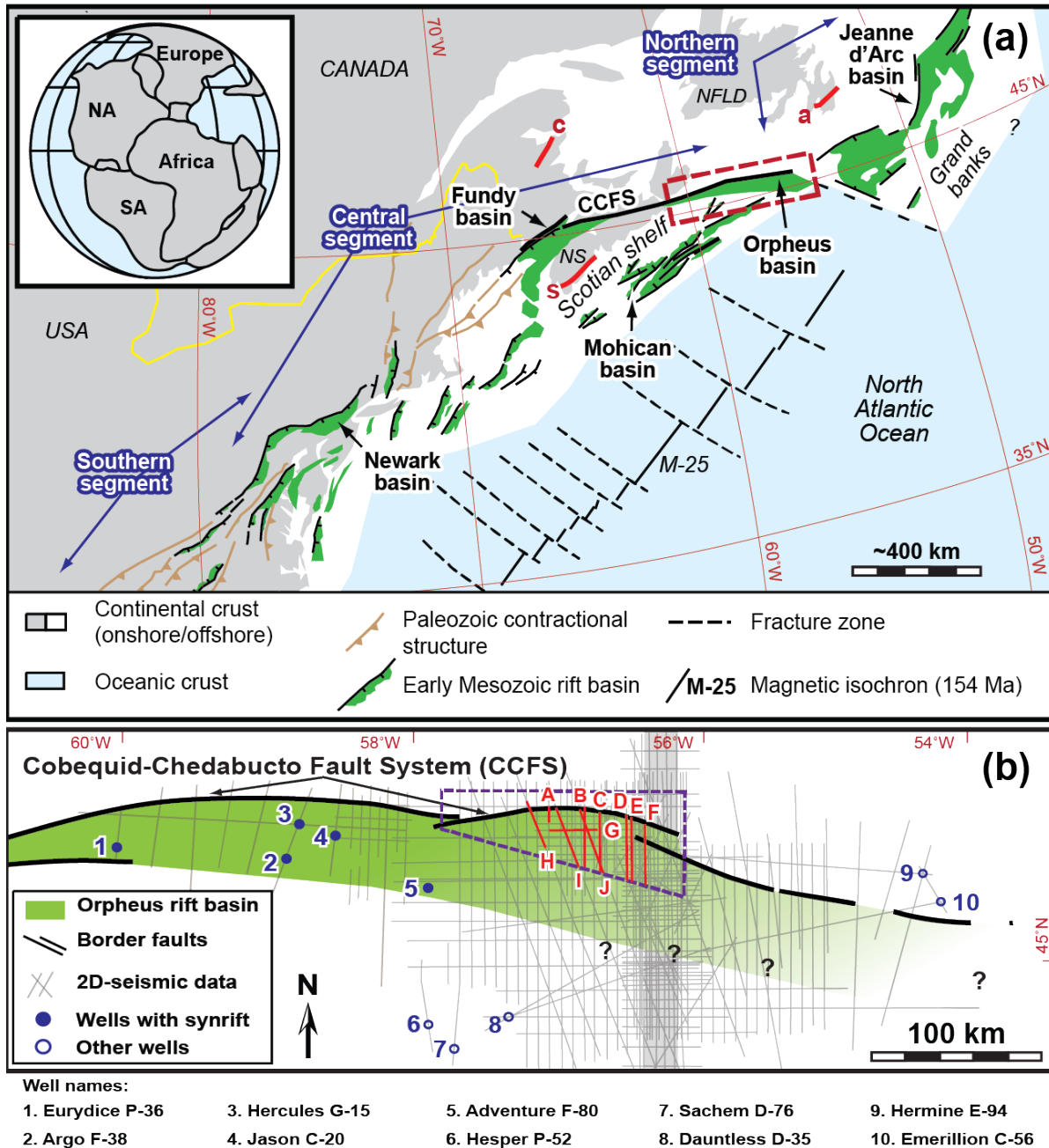

Figure 1. (a) *Regional map of eastern North America showing major Paleozoic contractional structures, early Mesozoic rift basins, and tectonic features (modified from Withjack et al., 2012). Yellow line shows boundary between Canada and the United States of America. Dashed red box shows approximate location of area in Figure 1b. Inset map shows Pangean*

*supercontinent during Late Triassic (after Olsen, 1997). NA: North America; SA: South America; NS: Nova Scotia; NFLD: Newfoundland. Thick black lines are Cobequid-Chedabucto fault system (CCFS). Red lines are select outcrops of intrusive rocks of Central Atlantic Magmatic Province (CAMP) near study area, a: Avalon dike; c: Caraquet dike; s: Shelburne dike. (**b**) Location map of Orpheus rift basin showing seismic and well data used in this study. Dashed polygon indicates focus area shown in Figures 2 and 9. Red, labeled lines are seismic profiles presented in this paper.*

The Orpheus rift basin, located offshore Nova Scotia and Newfoundland, Canada, is the northernmost rift basin in the central segment of the ENAM rift system (Fig. 1a). Previous studies, using primarily well data from the western Orpheus rift basin, have identified synrift clastic and evaporitic sedimentary rocks, including massive and interbedded salt (MacLean and Wade, 1993; Tanner and Brown, 2003). To complement these studies from the western Orpheus basin, we have used borehole data and a dense-grid of high-quality 2D seismic-reflection lines (Figs. 1b, 2) to establish the tectonostratigraphic framework, characterize the basement-involved and detached structures, determine the timing of deformation, and identify large-scale depositional patterns in the eastern Orpheus basin. Specifically, this study addressed the following questions: 1) What is the basic geometry of the eastern Orpheus basin? 2) How does deformation vary temporally and spatially throughout the eastern Orpheus basin? What factors controlled the development of these deformation patterns? 3) Are the synrift rocks in the eastern Orpheus basin similar to those in the western Orpheus basin? If not, how do they differ, and what processes likely caused the spatial variability of the synrift strata? 4) How does the variability of the synrift strata affect the mechanical stratigraphy and deformation within the rift basin? Answers to these questions will lead to a better understanding of the development of the Orpheus basin and other rift basins of the ENAM rift system as well as the complex interplay between rift-related faulting, salt deposition, and salt flow during and after rifting.
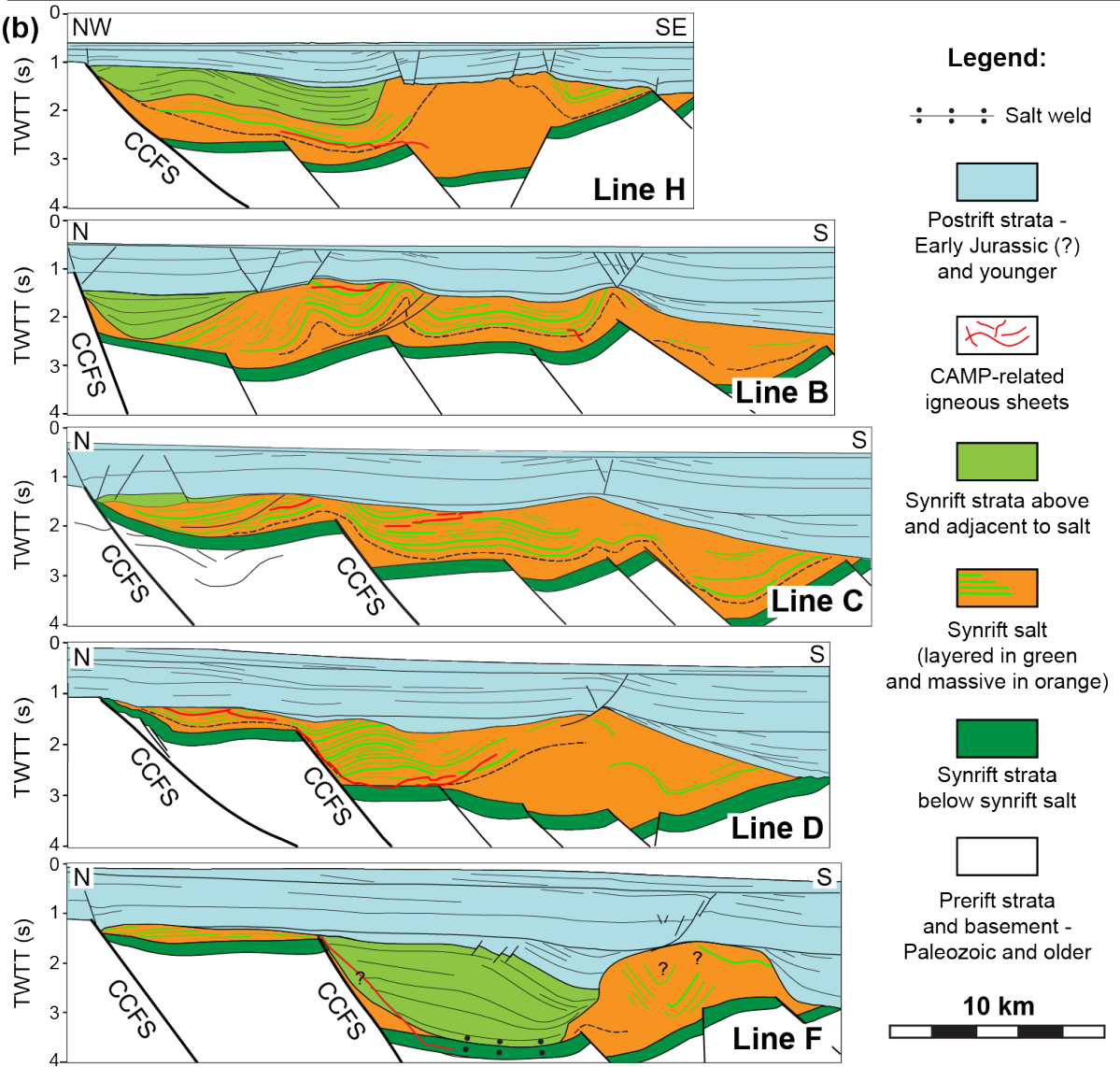
(a) CCFS ... Relay ramp of CCFS

57.5°W   57°W   56.5°W

45.5°N

2

3

4

Seconds

A

G

H

I

B   C   J   E   D   F

N

Border-fault segments

Basement-involved intrabasinal faults

10 km

(b)

NW   SE
0
1
2
3
4
TWTT (s)
CCFS
Line H

N   S
0
1
2
3
4
TWTT (s)
CCFS
Line B

N   S
0
1
2
3
4
TWTT (s)
CCFS   CCFS
Line C

N   S
0
1
2
3
4
TWTT (s)
CCFS   CCFS
Line D

N   S
0
1
2
3
4
TWTT (s)
CCFS   CCFS
?   ?   ?
Line F

Legend:

Salt weld

Postrift strata - Early Jurassic (?) and younger

CAMP-related igneous sheets

Synrift strata above and adjacent to salt

Synrift salt (layered in green and massive in orange)

Synrift strata below synrift salt

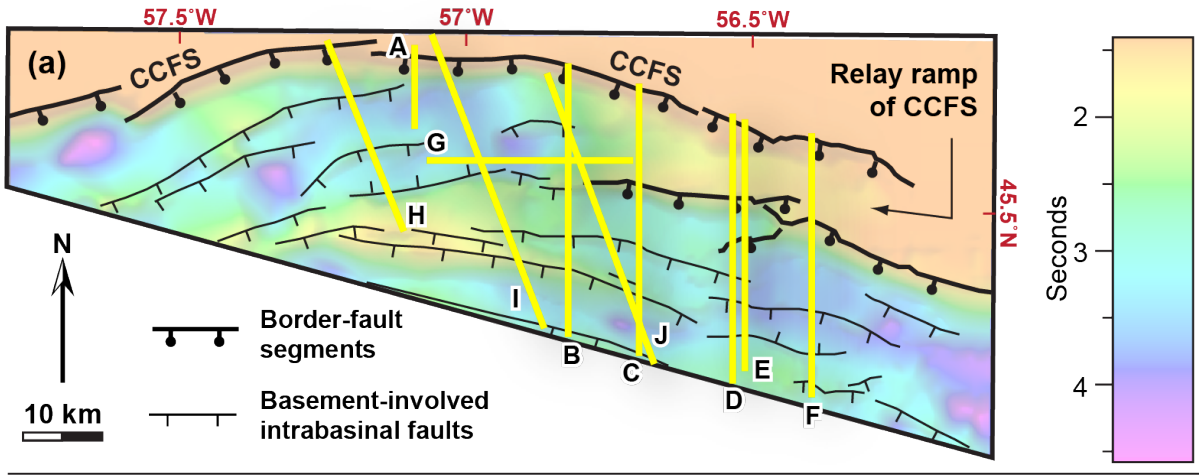Prerift strata and basement - Paleozoic and older

10 km

5

Figure 2. (a) *Time-structure map of base of synrift salt south of the border-fault system and top of basement north of the border-fault system, showing basement architecture of Orpheus rift basin. Note overlapping segments of border-fault system produced relay ramps. Color bar shows two-way travel time in seconds.* *(b)* *Cross sections through eastern Orpheus rift basin based on 2D seismic-reflection data. CCFS: Cobequid-Chedabucto fault system; CAMP: Central Atlantic Magmatic Province. Black dashed line in cross sections is approximate boundary between massive lower salt and layered upper salt. Seismic lines are displayed 1:1 assuming a velocity of 4.5 km/s.*

2. GEOLOGIC OVERVIEW OF THE ORPHEUS RIFT BASIN AND SURROUNDING REGION

As noted above, the Orpheus rift basin is part of the central segment of the ENAM rift system with rifting beginning by the Late Triassic and ceasing in the Early Jurassic when continental breakup occurred (e.g., Manspeizer, 1988; Manspeizer and Cousminer, 1988; Olsen, 1997; Withjack and Schlische, 2005; Olsen and Et-Touhami, 2008; Withjack et al., 2012). The Grand Banks region immediately to the north of the Orpheus rift basin is part of the northern segment of the ENAM rift system with rift onset by the Late Triassic but breakup occurring much later in the Cretaceous (Withjack and Schlische, 2005; Welsink and Tankard, 2012; Withjack et al., 2012).

In latest Triassic/earliest Jurassic time, a short-lived (< 1 my), but widespread, igneous event of the Central Atlantic Magmatic Province (CAMP) affected the entire ENAM rift system (Verati et al., 2007; Marzoli et al., 2011; Blackburn et al., 2013; Davies et al., 2017; Marzoli et al., 2019). The absolute age of CAMP is ~ 201 Ma based on isotopic dating of both intrusive and extrusive rocks (Verati et al., 2007; Marzoli et al., 2011; Blackburn et al., 2013; Davies et al., 2017; Marzoli et al., 2019). CAMP-related igneous activity included the intrusion of diabase sheets and dikes and the eruption of basalts. In the region surrounding the Orpheus basin (Fig. 1a), CAMP-related igneous rocks include the North Mountain Basalt in the Fundy rift basin

(Dostal and Greenough, 1992; Olsen and Et-Touhami, 2008; Cirilli et al., 2009; Jourdan et al., 2009) and the Shelburne (Pe-Piper et al., 1992; Dostal and Durning, 1998; Dunn et al., 1998), Caraquet (Pe-Piper et al., 1992; Dostal and Durning, 1998), and Avalon dikes (Pe-Piper et al., 1992). CAMP-related basalts are also present in nearby wells from the region between the Fundy and Orpheus rift basins (White et al., 2017), in the Mohican rift basin on the Scotian Shelf (Weston et al., 2012), and in the Jeanne d'Arc rift basin of the Grand Banks region (Pe-Piper et al., 1992).

After rifting and breakup, the region underwent thermal subsidence with intermittent faulting, uplift, and erosion, allowing accumulation of a thick postrift sequence consisting of mainly marine sedimentary rocks in a broad depression known as the Scotian basin (Wade and MacLean, 1990; MacLean and Wade, 1992; Wade et al., 1995). A breakup unconformity, a major erosional surface that marks the rift/drift transition, separates the synrift strata from the overlying postrift strata on the Scotian Shelf (Wade and MacLean, 1990; MacLean and Wade, 1992, 1993; Wade et al., 1995; Deptuck and Altheim, 2018). Despite the presence of the breakup unconformity in the region, the precise timing of continental breakup remains unclear. Early Jurassic synrift rocks (Sinemurian) are exposed in the adjacent ENAM Fundy rift basin (Olsen, 1997). Therefore, rifting continued into the Early Jurassic in the region. The age of the oldest postrift strata in the Scotian basin, however, is poorly constrained. Researchers initially assigned an Early Jurassic age (i.e., late Sinemurian-early Pliensbachian) for the oldest postrift strata in the Scotian basin (Barss et al., 1979; Wade and MacLean, 1990). Recent biostratigraphic studies (Weston et al., 2012; Ainsworth et al., 2016), however, were unable to confirm this Early Jurassic age. Well analysis from the Offshore Energy Technical Research Association (OETR) suggests that the oldest drilled postrift strata in the Orpheus region is late Middle Jurassic (i.e.,

Bathonian) (see Chapter 4 of OETR, 2014). However, seismic data from the Scotian Shelf suggest that Jurassic strata progressively onlap onto the breakup unconformity (Deptuck and Altheim, 2018), indicating that Early Jurassic postrift rocks may have accumulated in the deeper parts of the Scotian basin near the site of breakup. Information from the conjugate margin of northwest Morocco suggests that the oldest postrift rocks are Sinemurian/Pliensbachian in age (Medina, 1995; Hafid, 2000), indicating that the cessation of rifting, continental breakup, and the onset of drifting occurred in Early Jurassic time (Withjack et al., 2012).

Information about the synrift rocks within the Orpheus rift basin is limited. Fluvial clastic sedimentary rocks of Late Triassic age crop out near the western end of the Orpheus rift basin (Tanner and Brown, 1999). Five wells in the western part of the basin reached synrift rocks. Of these, only the Eurydice P-36 and Argo F-38 wells penetrated a significant part of the synrift section; the other three wells (i.e., Adventure F-80, Hercules G-15, and Jason C-20 wells) drilled only the uppermost part (MacLean and Wade, 1992, 1993). In the Argo F-38 and Eurydice P-36 wells (Figs. 1b, 3), continental red sandstones and shales of the Eurydice Formation were present (MacLean and Wade, 1992; Wade et al., 1995; Tanner and Brown, 2003). These are dated as latest Triassic to earliest Jurassic (i.e., Rhaetian-Hettangian) (Bujak and Williams, 1977; Barss et al., 1979), but seismic-reflection data indicate that an estimated 2 km of older synrift rocks underlie the drilled section in the Eurydice P-36 well (Wade and MacLean, 1990; Tanner and Brown, 2003). In the Argo F-38 and Eurydice P-36 wells, salt of the Argo Formation overlies the Eurydice Formation (MacLean and Wade, 1992; Wade et al., 1995; Tanner and Brown, 2003) (Fig. 3). In these wells, the Argo Formation consists of a lower massive salt unit and an upper unit of interbedded salt and shale. The amount of shale varies within the upper unit, ranging from shale-rich (shale-to-salt ratio of ~3:1) in the Eurydice P-36 well to relatively shale-poor
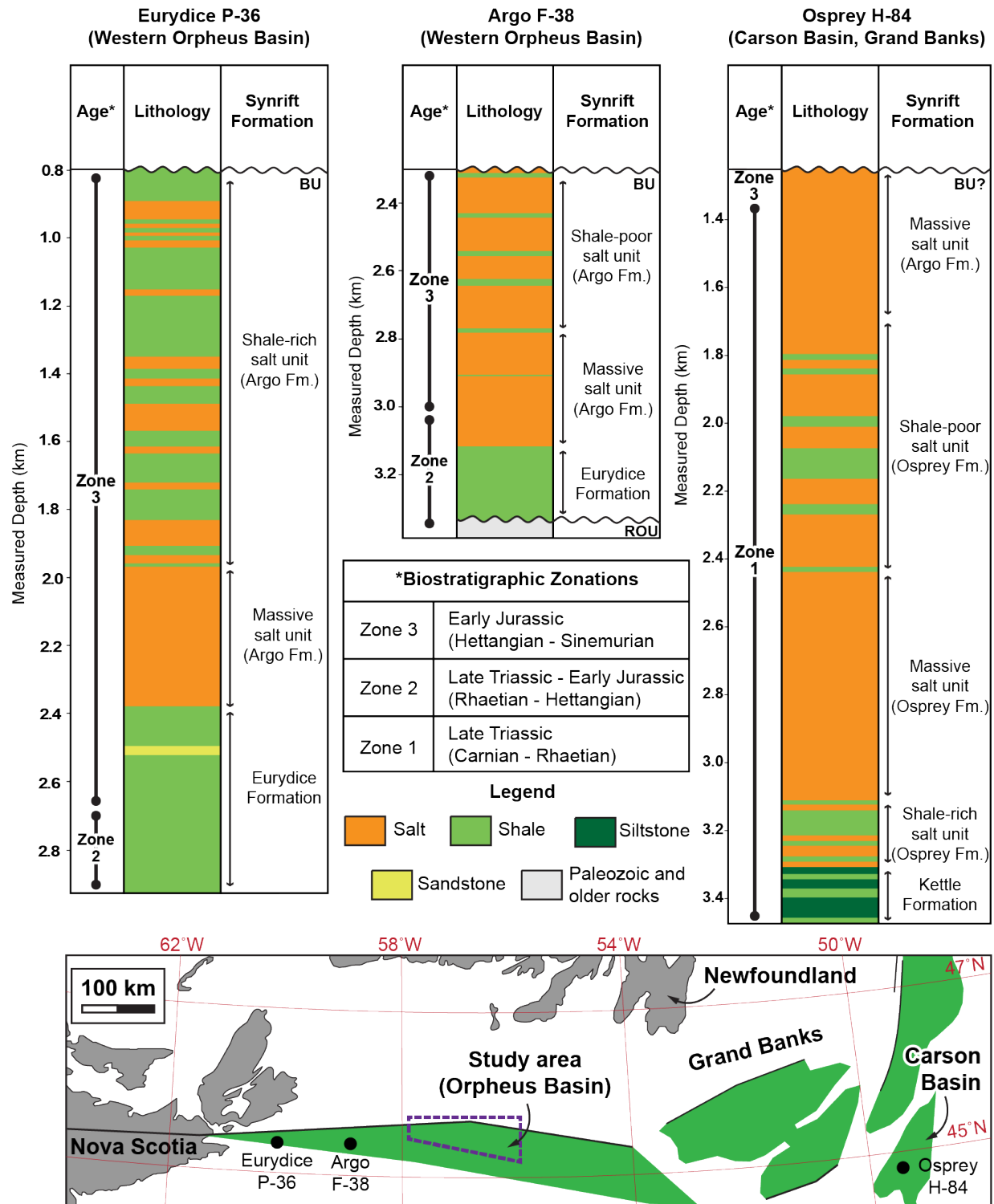
Figure 3. *Synrift lithology from Eurydice P-36 (left) and Argo F-38 (middle) wells of the western Orpheus basin, and Osprey H-84 (right) well of the Carson basin in the Grand Banks showing the temporal and lateral variability of the synrift salt surrounding the study area. In all wells, clastic sedimentary rocks (i.e., the Eurydice and Kettle formations in the western Orpheus and*

Carson basins, respectively) underlie Late Triassic-Early Jurassic synrift salt. In the western Orpheus rift basin, the age of the synrift salt is mostly Early Jurassic consisting of a lower massive salt and upper interbedded salt of the Argo Formation. The composition of the upper Argo Formation varies in both wells with more interbedded salt-shale in the Eurydice P-36 well and less interbedded salt-shale in the Argo F-38 well. The older synrift salt of Late Triassic age (i.e., Osprey Formation) in the Carson basin consists of massive salt and interbedded salt-shale units. Note that the study area is located between the Eurydice P-36 and Argo F-38 wells in the western Orpheus basin and the Osprey H-84 well in the Carson basin. Age is based on biostratigraphic zonation by Barss et al. (1979). BU: Breakup unconformity; ROU: Rift-onset unconformity. (Adapted from Holser et al., 1988; MacLean and Wade, 1993).

(shale-to-salt ratio of ~1:10) in the Argo F-38 well (Fig. 3). The palynological age of the Argo Formation in the western Orpheus rift basin is Early Jurassic (Hettangian-Sinemurian) (Bujak and Williams, 1977; Barss et al., 1979).

No wells have penetrated the synrift section in the eastern Orpheus rift basin, but data from the surrounding ENAM rift basins and the conjugate margin of Morocco provide additional information about the possible ages and lithologies of the fill within the eastern part of the basin. Synrift rocks from the Scotian Shelf and Grand Banks region, directly south and north of the eastern Orpheus rift basin (Figs. 1a, 3), respectively, include red sandstones and shales of Late Triassic age which underlie and/or interfinger with synrift salt of Late Triassic to Early Jurassic age (Tankard et al., 1989; Wade and MacLean, 1990; MacLean and Wade, 1992; Welsink and Tankard, 2012; Weston et al., 2012). Similarly, synrift strata on the conjugate margin of Morocco consist of Late Triassic redbeds and Late Triassic-Early Jurassic synrift salt (Hafid, 2000; Hafid et al., 2006; Tari and Jabour, 2013; Saura et al., 2014; Martin-Martin et al., 2017). In the Scotian and Grand Banks regions, some authors have subdivided the synrift salt into a lower unit of Late Triassic age called the Osprey Formation (Barss et al., 1979; Jansa et al., 1980; Holser et al., 1988; Manspeizer, 1988) and an upper unit of Late Triassic to Early Jurassic age called the Argo Formation (Holser et al., 1988; Sinclair, 1995; Sinclair et al., 1999) (e.g., Osprey

H-84 well, Fig. 3). Others, however, refer to the entire salt package from the Scotian Shelf and Grand Banks regions as the Argo Formation (e.g., Sinclair, 1993; Weston et al., 2012). In this study, we refer to the synrift salt in the Orpheus rift basin, regardless of its age, as the Argo Formation.

3.   SEISMIC-REFLECTION AND WELL DATA

This study uses more than 13,500 km of time-migrated, 2D seismic-reflection profiles that cover >30,000 km^2 of offshore Nova Scotia and Newfoundland, Canada (Fig. 1b). These industry lines, acquired in the 1980s, 1990s, and 2000s, were processed using standard methods such as data resampling, bad-trace editing, deconvolution, velocity analysis, and the Kirchoff pre-stack time migration (Yilmaz, 1987). In 2006, the Geological Survey of Canada reprocessed some key seismic profiles (acquired in 1984-1985), suppressing multiples and improving seismic imaging. In some seismic profiles (Fig. 4), however, peg-leg multiples associated with the water column still occur below ~2 s two-way travel time (TWTT). These multiples, commonly associated with high-amplitude reflections, can obscure the primary seismic reflections at depth. The western part of the Orpheus rift basin has relatively low-quality seismic-reflection profiles (acquired in the 1980s) with line spacing of 15-20 km, whereas the eastern part of the basin has high-quality data (acquired mostly from 1998 to 2002) with line spacing of 2-5 km. The 2D seismic-reflection data have a sampling interval of 2-4 milliseconds and a record length of 8-12 seconds two-way travel time (TWTT).

Ten boreholes in the Orpheus rift basin provide well data such as rock cuttings, gamma-ray logs, and check-shot velocities (MacLean and Wade, 1993)(Fig. 1b). As mentioned previously, five of the ten wells drilled into the Late Triassic-Early Jurassic synrift section.
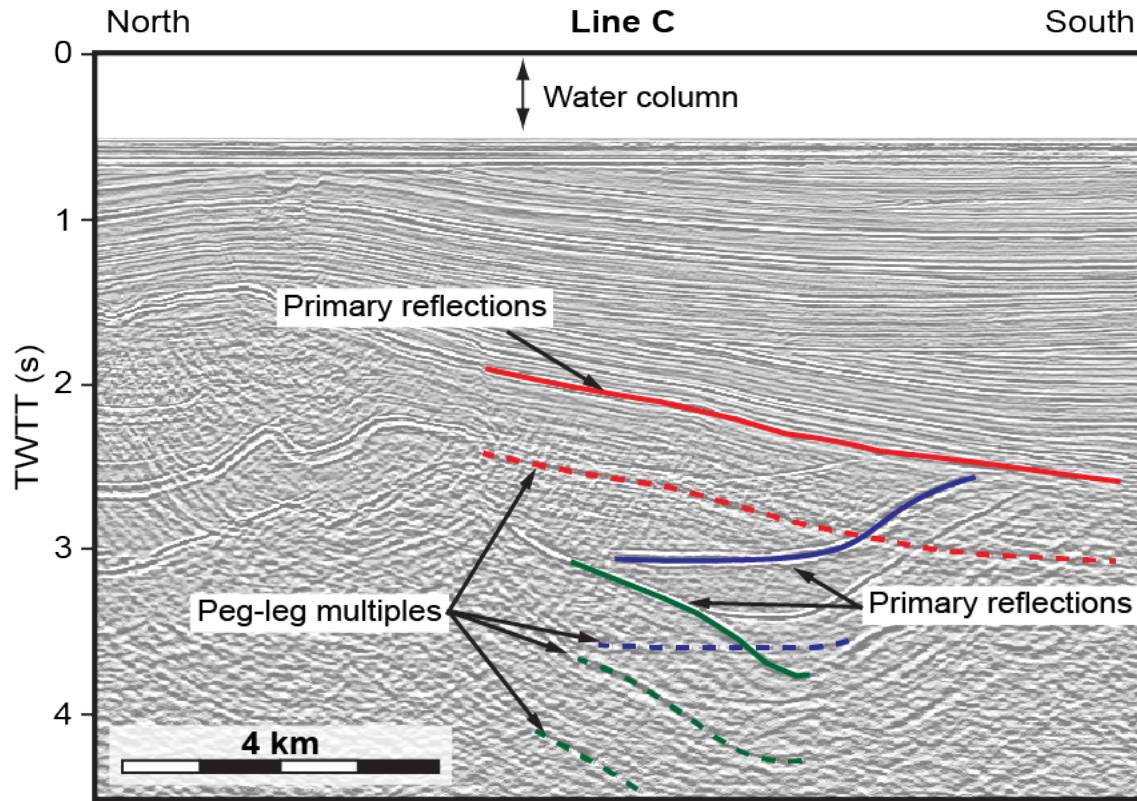
11

Figure 4. *Southern part of Line C (see Fig. 1b for location and Fig. 5 for interpretation) showing the presence of peg-leg multiples (dashed red, blue, and green lines) that mimic the primary reflections above them (solid red, blue, and green lines). Seismic line is displayed 1:1 assuming a velocity of 4.5 km/s.*

Only the Eurydice P-36 and Argo F-38 wells penetrated both the synrift Eurydice and Argo formations, whereas the other three wells only drilled the uppermost preserved part of the Argo Formation (i.e., Adventure F-80, Hercules G-15, and Jason C-20 wells). The remaining wells either drilled the footwall area outside the basin or bottomed in the Middle Jurassic or younger postrift section (MacLean and Wade, 1992, 1993). To date the seismic horizons, we used the biostratigraphic data from seven wells (i.e., Argo F-38, Eurydice P-36 wells, Emerillon C-56, Hermine E-94, Sachem D-76, Hesper P-52, and Dauntless D-35 wells) (Barss et al., 1979; Ascoli, 1988). The sonic-log and check-shot velocity data in these wells permit well-to-seismic

correlation using synthetic seismograms (MacLean and Wade, 1993). Using the check-shot velocity data from the Eurydice P-36 and Argo F-38 wells and the interval velocities from three seismic lines in the study area, we estimated that the synrift section in the study area has an average seismic velocity of ~4.5 km/s (Table 1). We used this value to display the seismic lines with approximately no vertical exaggeration at the level of the synrift section.
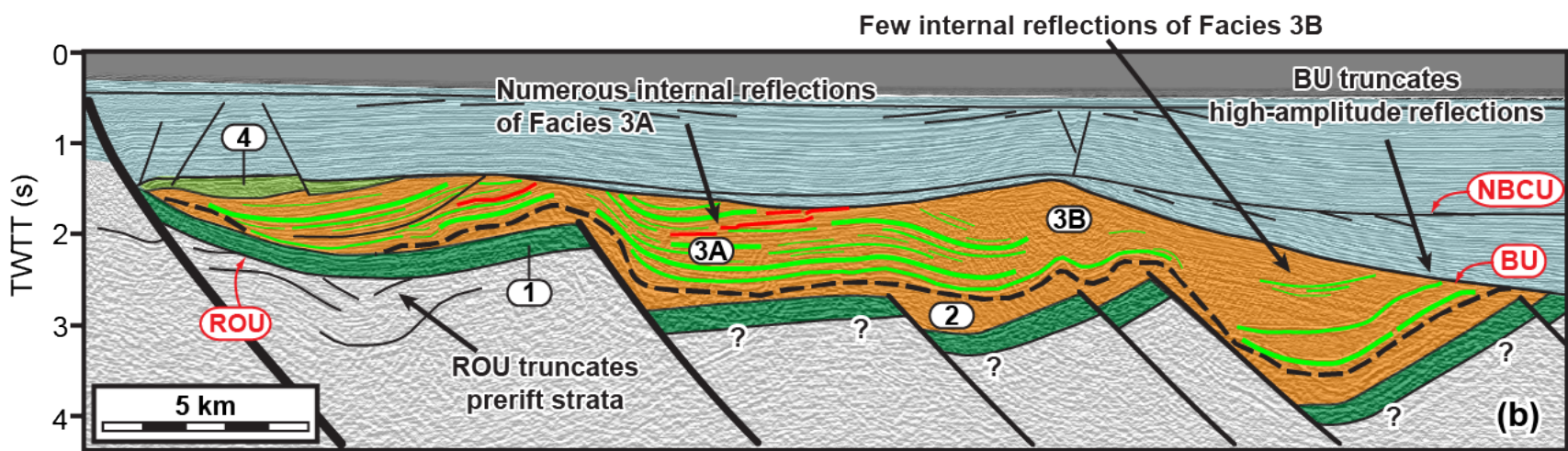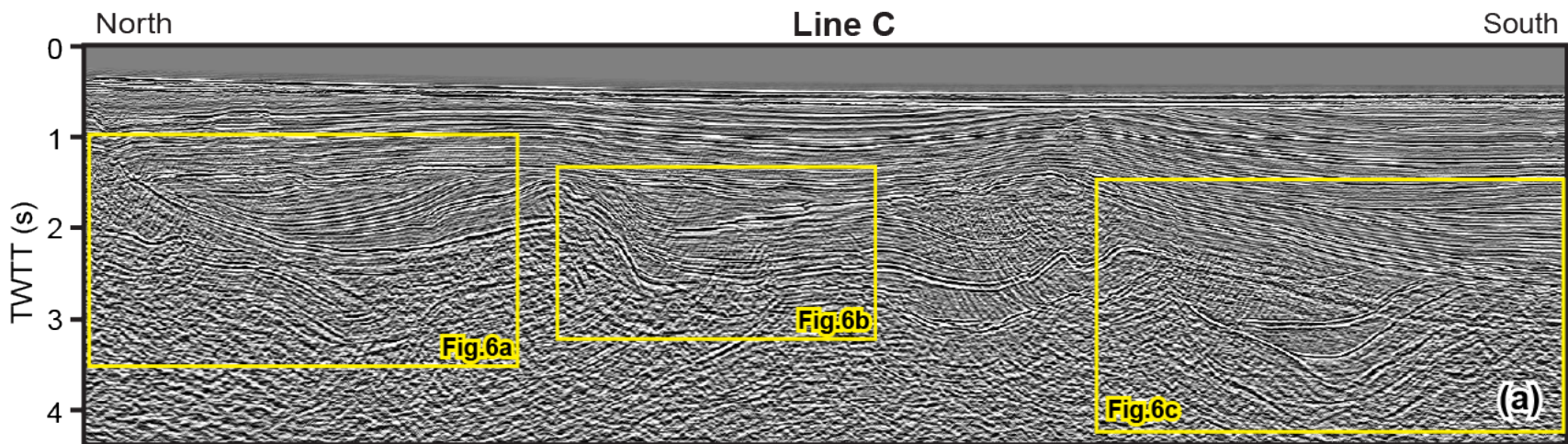
Table 1. Interval velocities of postrift and synrift packages in the Orpheus rift basin based on check-shot velocities from two wells and interval velocities from three seismic-reflection profiles. See Figure 1b for well and seismic line locations and text for descriptions of postrift and synrift packages.

Seismic Package	Check-shot Interval Velocity (km/s)		Seismic Interval Velocity (km/s)			Average Interval Velocity (km/s)
	Eurydice P-36	Argo F-38	Line H	Line I	Line J	
Postrift	2.8	3.0	2.4	2.6	2.5	2.6
Synrift	4.0	4.3	4.7	4.4	4.7	4.4

4. SEISMIC OBSERVATIONS

4.1. Tectonostratigraphic framework of eastern Orpheus rift basin

Using the dense grid of 2D seismic profiles and the available well data from the study area, we identified three tectonostratigraphic packages (i.e., prerift, synrift, and postrift) and three major angular unconformities (i.e., rift-onset, breakup, and near-base Cretaceous) in the eastern Orpheus rift basin (Fig. 5). Our tectonostratigraphic framework is similar to those established by Wade and Maclean (1990) and Maclean and Wade (1992). The deepest and oldest package in the study area is the prerift package. It is either seismically chaotic, likely representing crystalline basement, or it consists of folded reflections, likely representing the folded Paleozoic rocks as,

Line C

North

South

(a)

Fig.6a

Fig.6b

Fig.6c

TWTT (s)

Few internal reflections of Facies 3B

Numerous internal reflections
of Facies 3A

BU truncates
high-amplitude reflections

NBCU

BU

3A

3B

4

ROU

1

2

ROU truncates
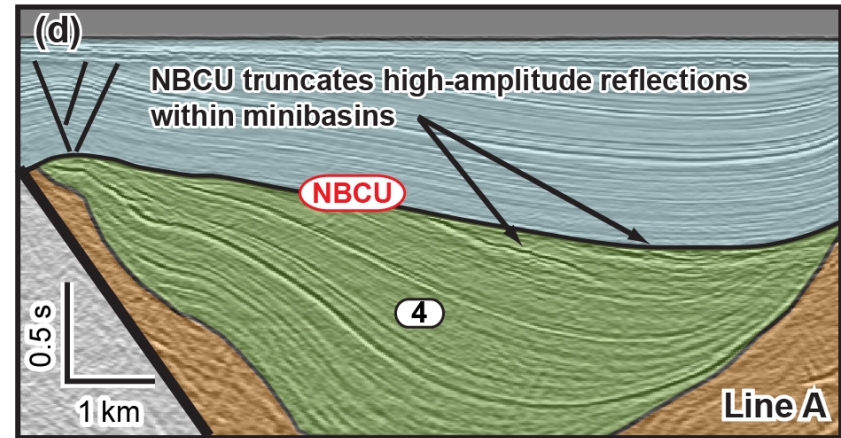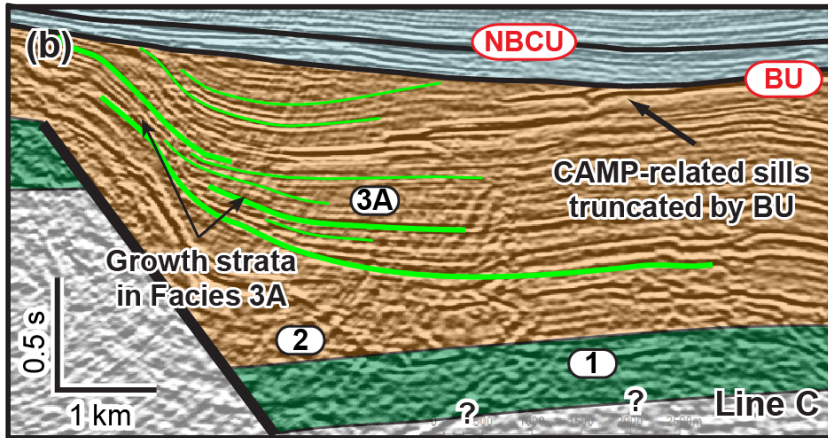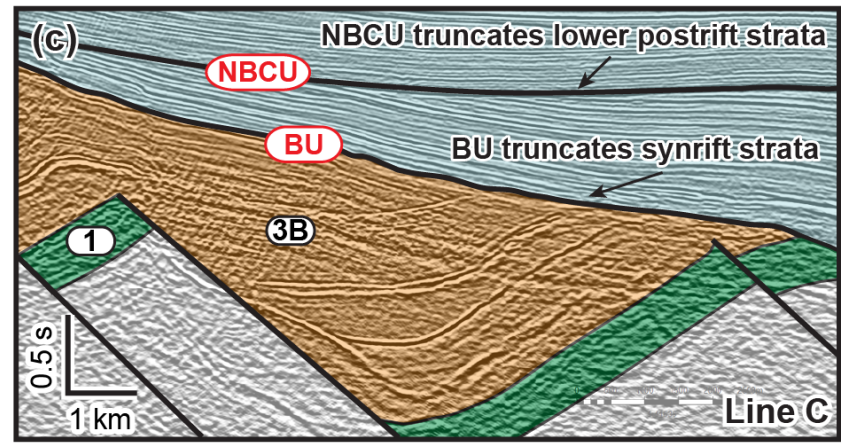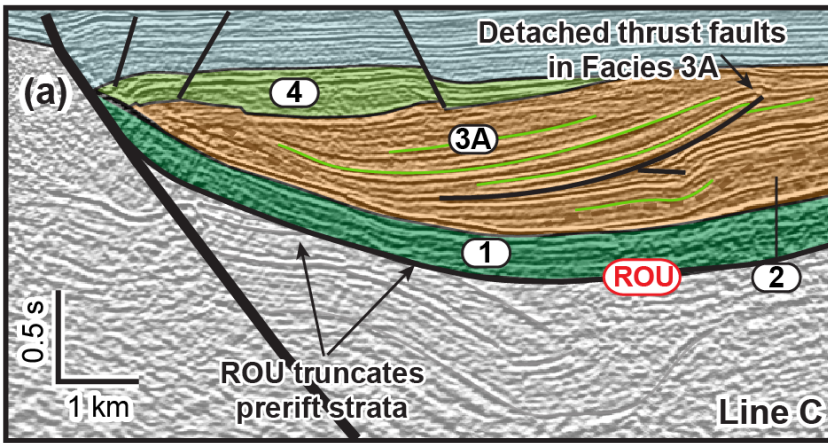prerift strata

5 km

(b)

TWTT (s)

Synrift strata below synrift salt	Synrift strata above and adjacent to salt	Postrift strata - Early Jurassic (?) and younger
Prerift strata and basement - Paleozoic and older	Synrift salt (layered in green, massive in orange)	CAMP-related igneous sheets

1

*Figure 5. Uninterpreted (**a**) and interpreted (**b**) versions of Line C (see Fig. 1b for location).*
Deepest tectonostratigraphic package (transparent white) includes prerift strata and basement.
Rift-onset unconformity (ROU) truncates folded prerift strata. Shallowest package (transparent
blue) is postrift strata. It is above the breakup unconformity (BU) and includes the near-base
Cretaceous unconformity (NBCU). Middle package includes synrift strata with four distinct
seismic units: Unit 1 (synrift strata below salt), Unit 2 (lower synrift massive salt), Unit 3 (upper
synrift salt), and Unit 4 (synrift strata above or adjacent to synrift salt). Note that Unit 3 has two
distinct facies: Facies 3A contains numerous well-imaged internal reflections (orange with
bright green layers), whereas Facies 3B is mostly transparent (orange) with few internal
reflections (green). Black dashed line is approximate boundary between Units 2 and 3. Red lines
are high-amplitude reflections interpreted as igneous sheets associated with CAMP, the Central
Atlantic Magmatic Province. TWTT: Two-way travel time. Yellow boxes in Figure 5a give
locations of seismic sections enlarged in Figure 6. Seismic line is displayed 1:1 assuming a
velocity of 4.5 km/s.

for example, encountered in the Hermine E-94 well (Wade and MacLean, 1990; MacLean and

Wade, 1993). An angular rift-onset unconformity (ROU) truncates the folded prerift strata and

separates them from the overlying synrift strata (Fig. 6a).

The rift-onset unconformity (ROU) defines the base of the synrift package of the eastern

Orpheus rift basin, whereas the angular breakup unconformity (BU) and the near-base

Cretaceous unconformity (NBCU) define the top of the synrift package in the south and north,

respectively (Figs. 6c-d). The basement-involved faults of the Cobequid-Chedabucto border-fault

system (CCFS) form the northern boundary of the synrift package (Fig. 2b). The thickness of the

synrift package varies considerably in the study area, from < 1 km near the border-fault system

to locally > 4.5 km (Fig. 2b). Reflections within the synrift package have highly variable

geometries (Fig. 7). In the following sections, we describe the synrift package of the eastern

Orpheus rift basin in greater detail.

The postrift package consists mainly of parallel-to-subparallel, continuous reflections that

are gently to moderately folded. The near-base Cretaceous unconformity (NBCU), a major

unconformity proposed by Weston et al. (2012) based on biostratigraphic data from the Scotian

(a) Detached thrust faults in Facies 3A — 4 — 3A — 1 — ROU — 2 — ROU truncates prerift strata — 0.5 s — 1 km — Line C

(b) NBCU — BU — 3A — Growth strata in Facies 3A — CAMP-related sills truncated by BU — 2 — 1 — ? — ? — 0.5 s — 1 km — Line C

(c) NBCU truncates lower postrift strata — NBCU — BU — BU truncates synrift strata — 1 — 3B — 0.5 s — 1 km — Line C

(d) NBCU truncates high-amplitude reflections within minibasins — NBCU — 4 — 0.5 s — 1 km — Line A

Synrift strata below synrift salt

Synrift strata above and adjacent to salt

Prerift strata and basement - Paleozoic and older

Synrift salt (layered in green, massive in orange)

Postrift strata - Early Jurassic (?) and younger

32

33 *Figure 6. Seismic lines showing detailed structural and stratigraphic features of prerift, synrift,*
34 *and postrift sections in the eastern Orpheus rift basin. Synrift package consists of four units:*
35 *Unit 1 (synrift presalt), Unit 2 (lower part of synrift salt), Unit 3 (upper part of synrift salt), and*
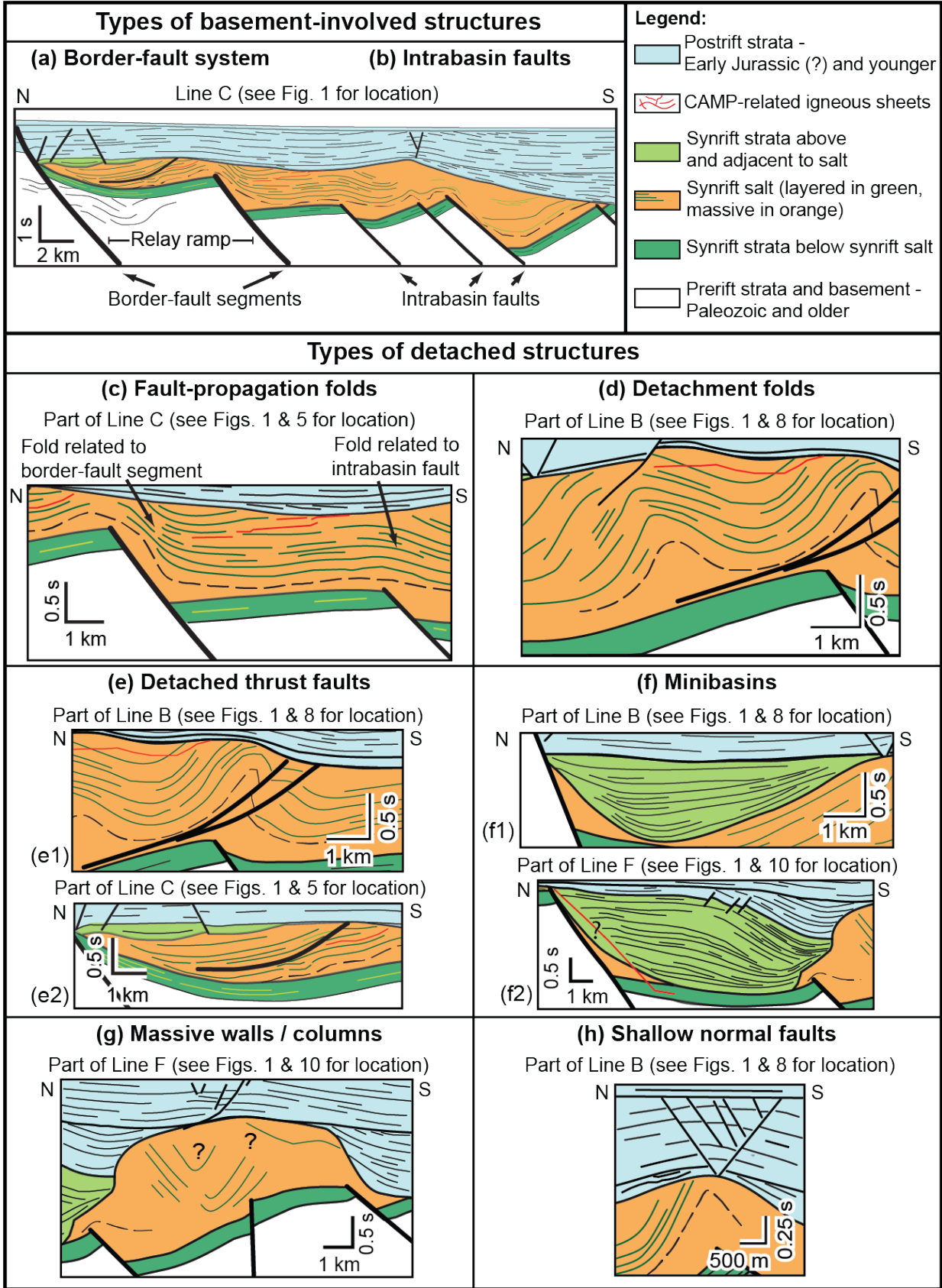36 *Unit 4 (minibasin or synrift suprasalt). (a) Northern part of Line C (Fig. 5) showing truncation*
37 *of folded prerift strata by rift-onset unconformity (ROU). Also note the presence of detached*
38 *thrust fault within Facies 3A. (b) Middle part of Line C (Fig. 5) showing growth strata*
39 *associated with Facies 3A. (c) Southern part of Line C (Fig. 5) showing breakup (BU) and near-*
40 *base Cretaceous unconformities (NBCU) that truncate synrift and lower postrift strata,*
41 *respectively. (d) Synrift strata above and/or adjacent to salt (i.e., minibasin) on Line A (Fig. 1b*
42 *for location). Also note truncation of high-amplitude reflections interpreted as CAMP-related*
43 *intrusives in minibasin by NBCU (near base Cretaceous unconformity). CAMP: Central Atlantic*
44 *Magmatic Province. Seismic lines are displayed 1:1 assuming a velocity of 4.5 km/s.*
45

46   basin, truncates the lower part of the postrift package in the southern part of the study area,

47   forming a clear angular unconformity and separating it from the overlying postrift strata (Figs. 5,

48   6c). Based on well correlations (Hermine E-94 and Emerillon C-56), the lower part of the postrift

49   package is Early (?) to Late Jurassic in age, whereas the upper part represents strata of Early

50   Cretaceous and younger age (MacLean and Wade, 1992; Weston et al., 2012; Ainsworth et al.,

51   2016). The near-base Cretaceous unconformity merges with the breakup unconformity in the

52   north (Fig. 5) and corresponds to the widespread Avalon unconformity described by Wade and

53   MacLean (1990) and MacLean and Wade (1992, 1993).

54

55   **4.2. Basement-involved structures in the eastern Orpheus rift basin**

56   Basement-involved structures in the study area include the border-fault system of the

57   Orpheus rift basin and numerous intrabasin faults (Figs. 2, 7a-b). In the study area, the border-

58   fault system consists of E-striking, right-stepping fault segments (Fig. 2a). Two large,

59   overlapping fault segments produce a major relay ramp (i.e., a monoclinal fold that connects the

60   footwall region to deeper parts of the hanging-wall basin) (Peacock and Sanderson, 1991;

61   Schlische et al., 2002; Withjack et al., 2002) (Fig. 2a). In cross-section view, the border-fault

Types of basement-involved structures

(a) Border-fault system   **(b) Intrabasin faults**

Line C (see Fig. 1 for location)

N — S

1 s / 2 km

Relay ramp

Border-fault segments   Intrabasin faults

Legend:

Postrift strata - Early Jurassic (?) and younger

CAMP-related igneous sheets

Synrift strata above and adjacent to salt

Synrift salt (layered in green, massive in orange)

Synrift strata below synrift salt

Prerift strata and basement - Paleozoic and older

Types of detached structures

(c) Fault-propagation folds

Part of Line C (see Figs. 1 & 5 for location)

Fold related to border-fault segment   Fold related to intrabasin fault

N — S

0.5 s / 1 km

(d) Detachment folds

Part of Line B (see Figs. 1 & 8 for location)

N — S

0.5 s / 1 km

(e) Detached thrust faults

Part of Line B (see Figs. 1 & 8 for location)

N — S

(e1)   0.5 s / 1 km

Part of Line C (see Figs. 1 & 5 for location)

N — S

(e2)   0.5 s / 1 km

(f) Minibasins

Part of Line B (see Figs. 1 & 8 for location)

N — S

(f1)   0.5 s / 1 km

Part of Line F (see Figs. 1 & 10 for location)

N — S

(f2)   0.5 s / 1 km

(g) Massive walls / columns

Part of Line F (see Figs. 1 & 10 for location)

N — S

? ?

0.5 s / 1 km

(h) Shallow normal faults

Part of Line B (see Figs. 1 & 8 for location)

N — S

500 m / 0.25 s

62

segments dip to the south, have normal separation, and offset the top of the prerift package (e.g., Figs. 2b, 5). Based on the kinematic linkage of the border-fault system of the Orpheus rift basin with that of the well-studied Fundy rift basin to the west (Fig. 1a), the border faults of the Orpheus rift basin likely had both normal and left-lateral components of slip during rifting that began by the Late Triassic and continued into the Early Jurassic (Withjack et al., 2009). Numerous basement-involved intrabasin faults with normal separation also developed during rifting in the Orpheus rift basin (Figs. 2a, 7b). In the study area, these intrabasin faults dip mainly toward the south and have less displacement than the border-fault segments.

4.3. Detached structures in the eastern Orpheus rift basin

Detached structures are abundant throughout the study area and provide clear evidence of major detachment levels and highly ductile strata (i.e., salt or overpressured shale) within the synrift package. Detached structures include forced folds, detachment folds, detached faults with normal and reverse separation, and massive walls and columns composed of intensely deformed strata (Fig. 7c-h).

Forced folds, consisting of monoclines with S-dipping limbs, developed above many basement-involved faults. They are a type of fault-propagation fold that forms where the upward transition from faulting to folding is abrupt, signifying the presence of a highly ductile layer at depth (Withjack and Callaway, 2000). The presence or absence of growth strata (i.e., beds

89   thinning toward the footwall) associated with these fault-propagation folds provides information

90   about the timing of folding and basement-involved faulting. For example, Line C (Figs. 5, 6b)

91   shows that the internal reflections of the synrift package converge and thin toward the footwall

92   of a border-fault segment, indicating syndepositional faulting during rifting. However, growth

93   strata are absent above the intrabasin faults in the south (Fig. 5), suggesting that some intrabasin

94   faulting occurred after the deposition of these synrift strata.

95   Detachment folds also developed within the synrift package. For example, Line B (Fig. 8)

96   shows moderately to tightly folded synrift strata above relatively undeformed fault blocks. This

97   decoupling between the shallow and deep structures suggests that a major detachment level

98   exists near the base of the synrift package (e.g., ~2.3 s TWTT on Line B). The detached

99   anticlines and synclines are subparallel to the border-fault system (Fig. 9b). Low-angle faults

100   (dip angle of < 30˚) with reverse separation offset the internal reflections of the synrift package

101   (Fig. 8). These thrust faults are listric, dip toward the north, and commonly sole out within a

102   major detachment level near the base of the synrift package. Other smaller faults with reverse

103   separation are present within the synrift package, suggesting that multiple detachment surfaces

104   exist internally within the synrift section (Fig. 6a). Based on a lack of growth beds, these

105   detached folds and faults formed after the deposition of the affected synrift strata. The truncation

106   of these folded and faulted strata by the breakup unconformity indicates that they formed before

107   and/or during the formation of the unconformity.

108   Detached structures also include tall walls and columns composed of intensely deformed

109   rocks exhibiting highly ductile behavior. The walls and columns overlie relatively undeformed

110   fault blocks (Fig. 10) and have heights reaching up to 2.5 seconds TWTT (~ 5.6 km with a

111   velocity of 4.5 km/s). In map view, the columns have diameters of ~ 5-10 km, whereas the walls
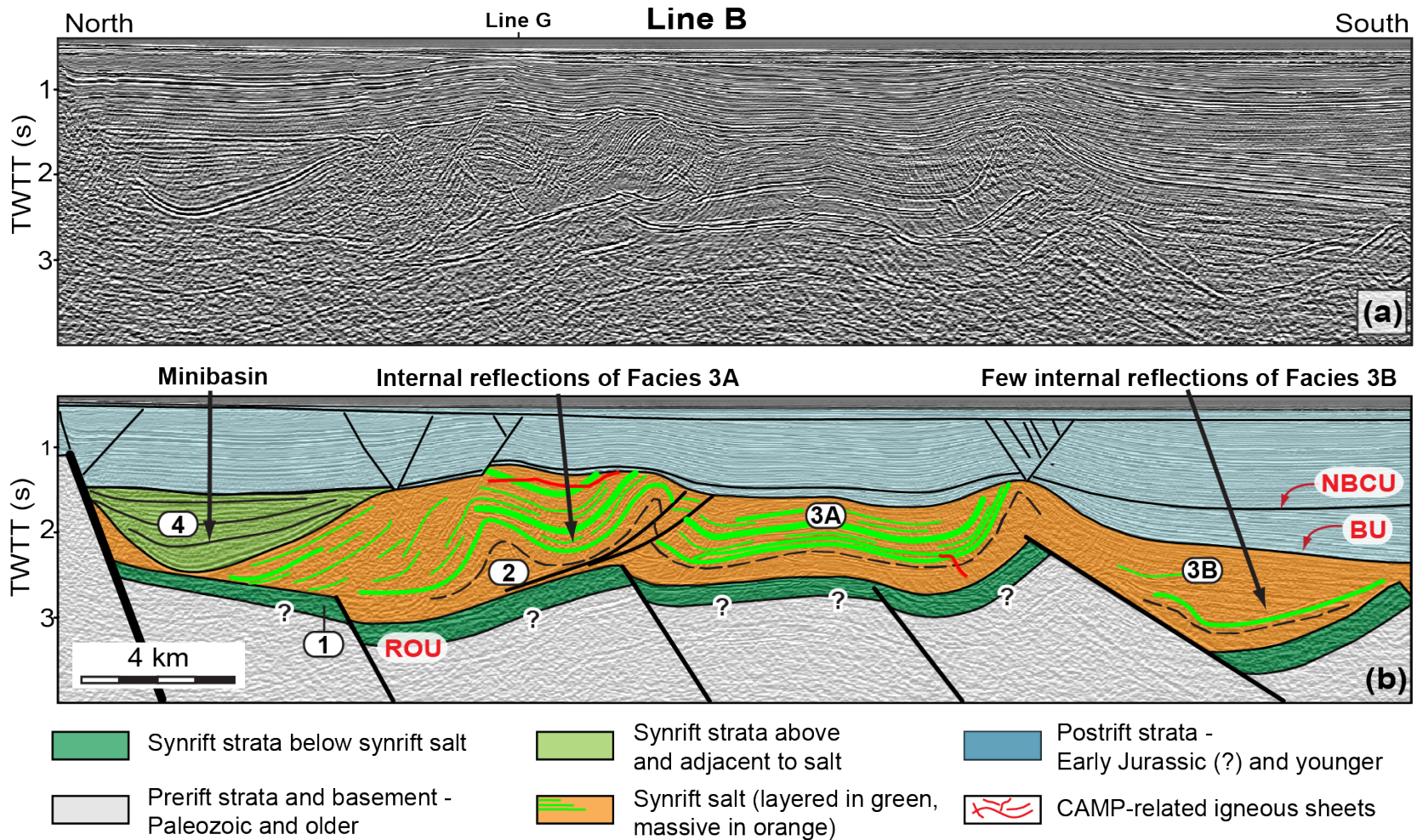
Figure 8. *Uninterpreted (a) and interpreted (b) versions of Line B (see Fig. 1b for location). Synrift package consists of four units: Unit 1 (synrift presalt), Unit 2 (lower part of synrift salt), Unit 3 (upper part of synrift salt), and Unit 4 (minibasin or synrift suprasalt). Note that Line B shows predominantly folded strata of Facies 3A. ROU: Rift-onset unconformity; BU: Breakup unconformity; NBCU: Near-base Cretaceous unconformity; CAMP: Central Atlantic Magmatic Province. TWTT: Two-way travel time. Black dashed line indicates approximate boundary between Units 2 and 3. Seismic line is displayed 1:1 assuming a velocity of 4.5 km/s.*

(a)

57.5°W   57°W   56.5°W

A

Salt is thin or absent
(minibasins)

Relay ramp

G

Salt columns

H

Seconds
2
3
4

I

Salt walls

B

J

C

D E F

Flat-top
salt body

45.5°N

(b)

57.5°W   57°W   56.5°W

Relay ramp

Seconds
2
3
4

Intrasalt folds, salt walls,
and border-fault system
have similar trend

45.5°N

(c)

57.5°W   57°W   56.5°W

Salt is thin or absent
(minibasin)

Facies 3B
dominant

Relay ramp

Facies 3A
dominant

N

Facies 3B dominant

10 km

45.5°N

Border-fault segment	Detached thrust fault	Detached syncline	Detached anticline

Figure 9. (a) Time-structure map of top Argo salt, (b) interpreted intrasalt structures, and (c) map showing distribution of Facies 3A (consisting of interbedded salt and shale), and Facies 3B (consisting of mostly massive rock salt with limited interbedded shale). Facies 3A is dominant near border-fault system and relay ramps. Salt is thin or absent in gray areas due to salt evacuation caused by sediment loading (i.e., minibasin formation). Yellow lines in Figure 9a show location of seismic lines described in text.

form ridges that are 5 to 10 km wide and more than 20 km long that are parallel or subparallel to the strike of the border-fault segments (Fig. 9a). Internal deformation within the walls and columns includes tightly folded and faulted beds (Fig. 10). The surrounding synrift and postrift strata thicken and/or thin toward the walls or columns (Figs. 10, 11), indicating that their growth occurred during and after rifting. Additionally, asymmetric synclines developed adjacent to the walls and columns (Fig. 10). Most of these synclines developed directly to the south of the border-fault system, creating depocenters that are 20 to 30 km long and 10 to 15 km wide (Fig. 9a). The thinning and/or thickening of strata within the synclines toward the adjacent walls and columns indicate that the formation of these folds was coeval with that of the walls and columns.

Shallow faults with normal separation are also present in the study area. These faults commonly offset the postrift strata and terminate at or offset the top of the synrift package (Fig. 8). Many of these faults formed as conjugate faults at the crest of anticlines that developed above the massive walls or columns (Fig. 8). Most shallow faults with normal separation are planar. However, some faults that penetrate deeper into the synrift package are listric (Fig. 12). None of these faults directly connects at depth with the basement-involved faults except for a few faults that terminate against the border-fault segments in the north (Fig. 8). The timing of shallow faulting is poorly constrained because of the lack of associated growth beds. However, these faults offset the near-base Cretaceous unconformity (NBCU) and strata above it; thus, they likely developed in Cretaceous or later time (i.e., well after rifting).

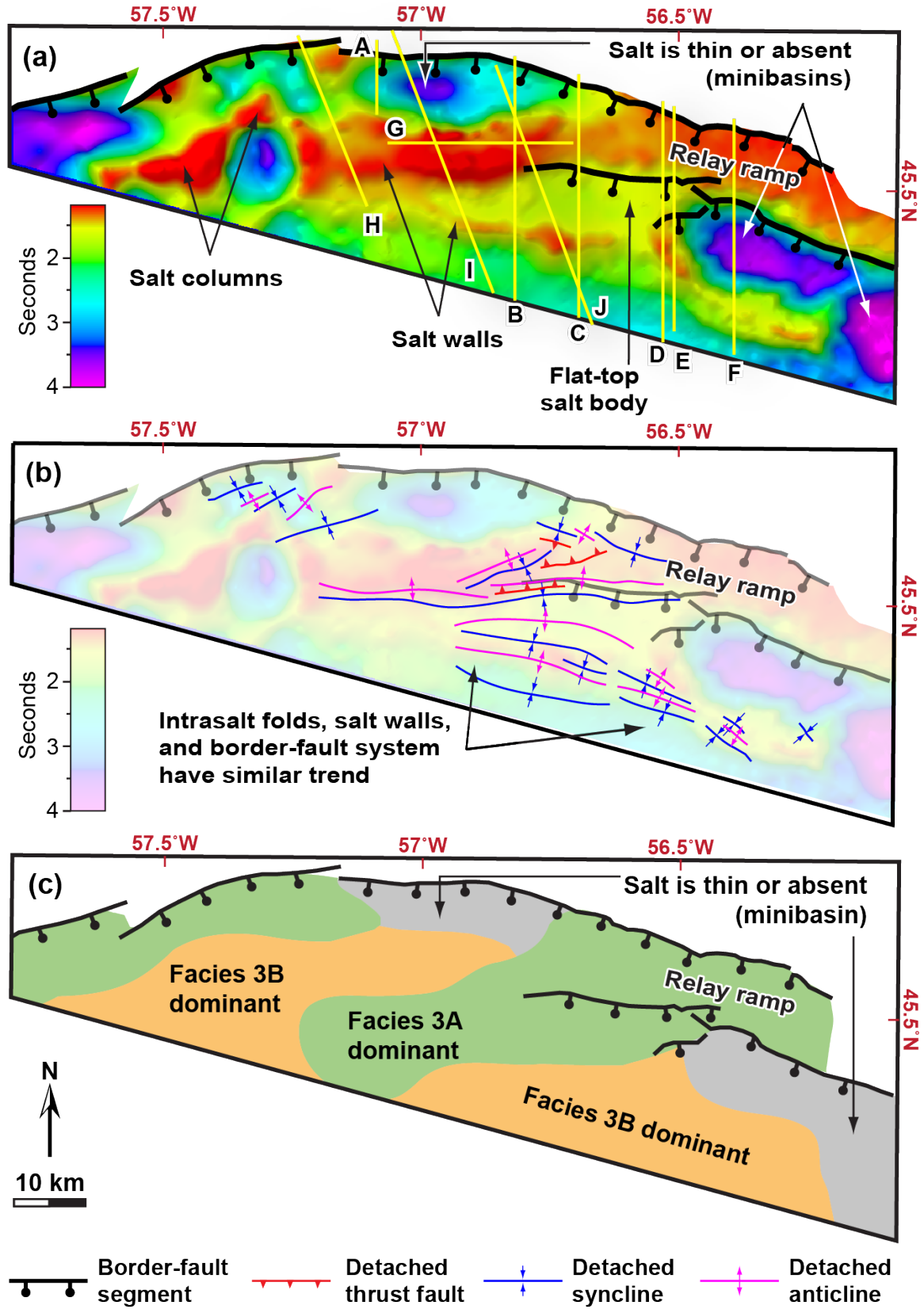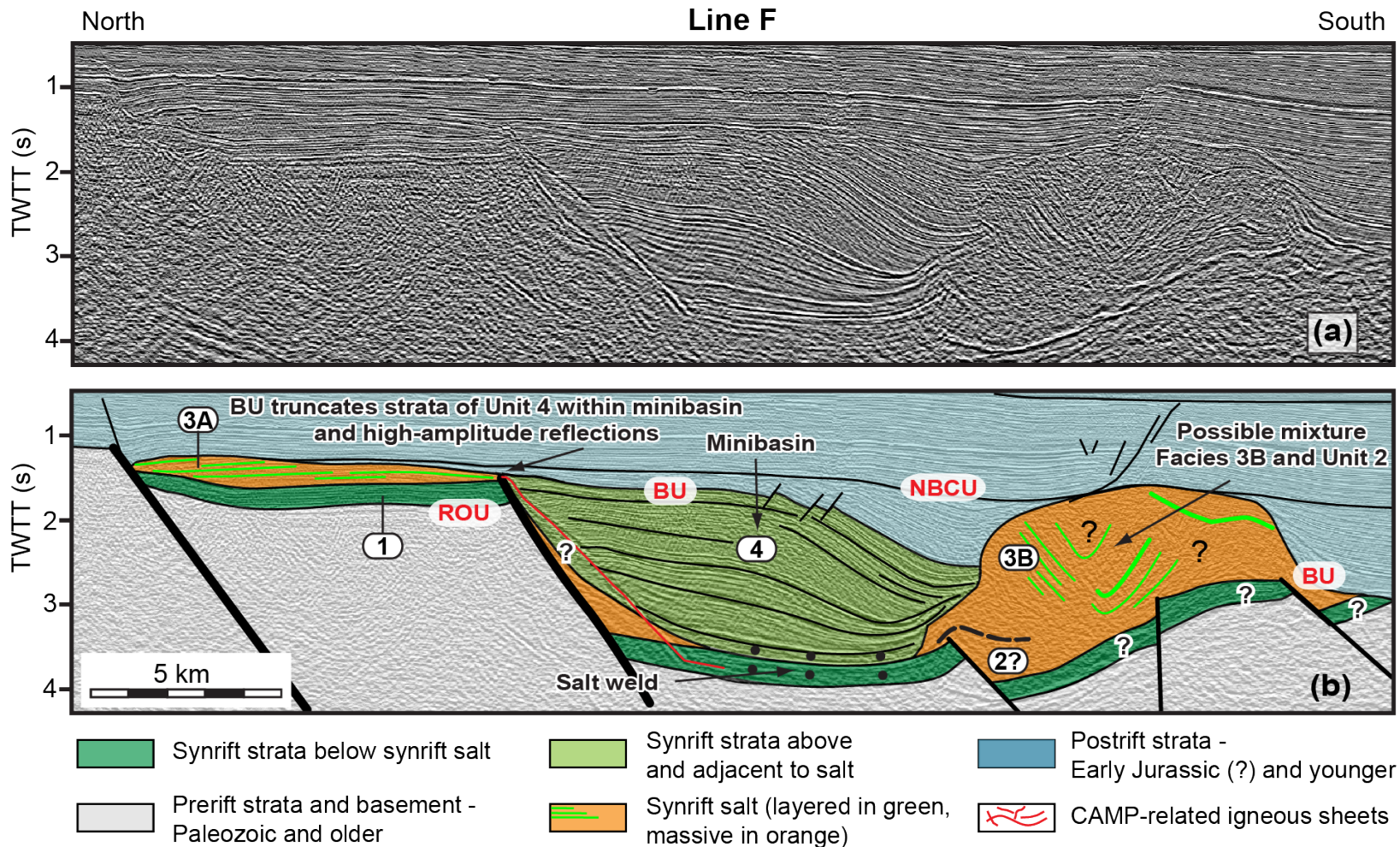**Figure 10.** Uninterpreted **(a)** and interpreted **(b)** versions of Line F (see Fig. 1b for location). Synrift package consists of four units: Unit 1 (synrift presalt), Unit 2 (lower part of synrift salt), Unit 3 (upper part of synrift salt), and Unit 4 (minibasin or synrift suprasalt). Salt wall of Unit 3/Facies B has a few, intensely deformed, internal reflections. ROU: Rift-onset unconformity; BU: Breakup unconformity; NBCU: Near-base Cretaceous unconformity; CAMP: Central Atlantic Magmatic Province. TWTT: Two-way travel time. Dashed black line indicates approximate boundary between Units 2 and 3. Seismic line is displayed 1:1 assuming a velocity of 4.5 km/s.

Figure 11. *Uninterpreted (a) and interpreted (b) versions of Line E (see Fig. 1b for location), showing truncation of high-amplitude reflections by breakup unconformity in minibasin. Synrift package consists of four units: Unit 1 (synrift presalt), Unit 2 (lower part of synrift salt), Unit 3 (upper part of synrift salt), and Unit 4 (minibasin or synrift suprasalt). ROU: Rift-onset unconformity; BU: Breakup unconformity; NBCU: Near-base Cretaceous unconformity; CAMP: Central Atlantic Magmatic Province. TWTT: Two-way*

travel time. Dashed black line indicates approximate boundary between Units 2 and 3. Seismic line is displayed 1:1 assuming a
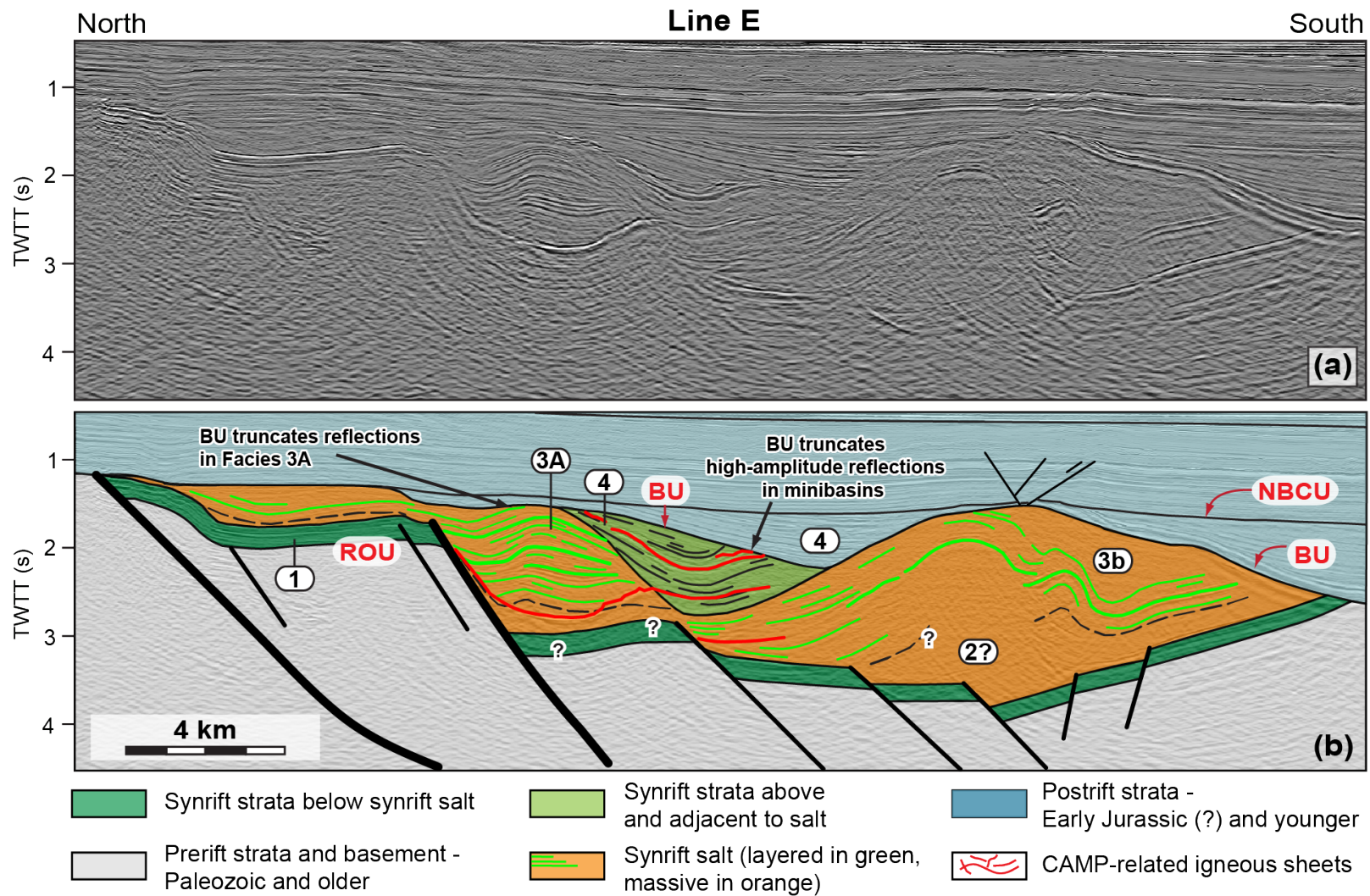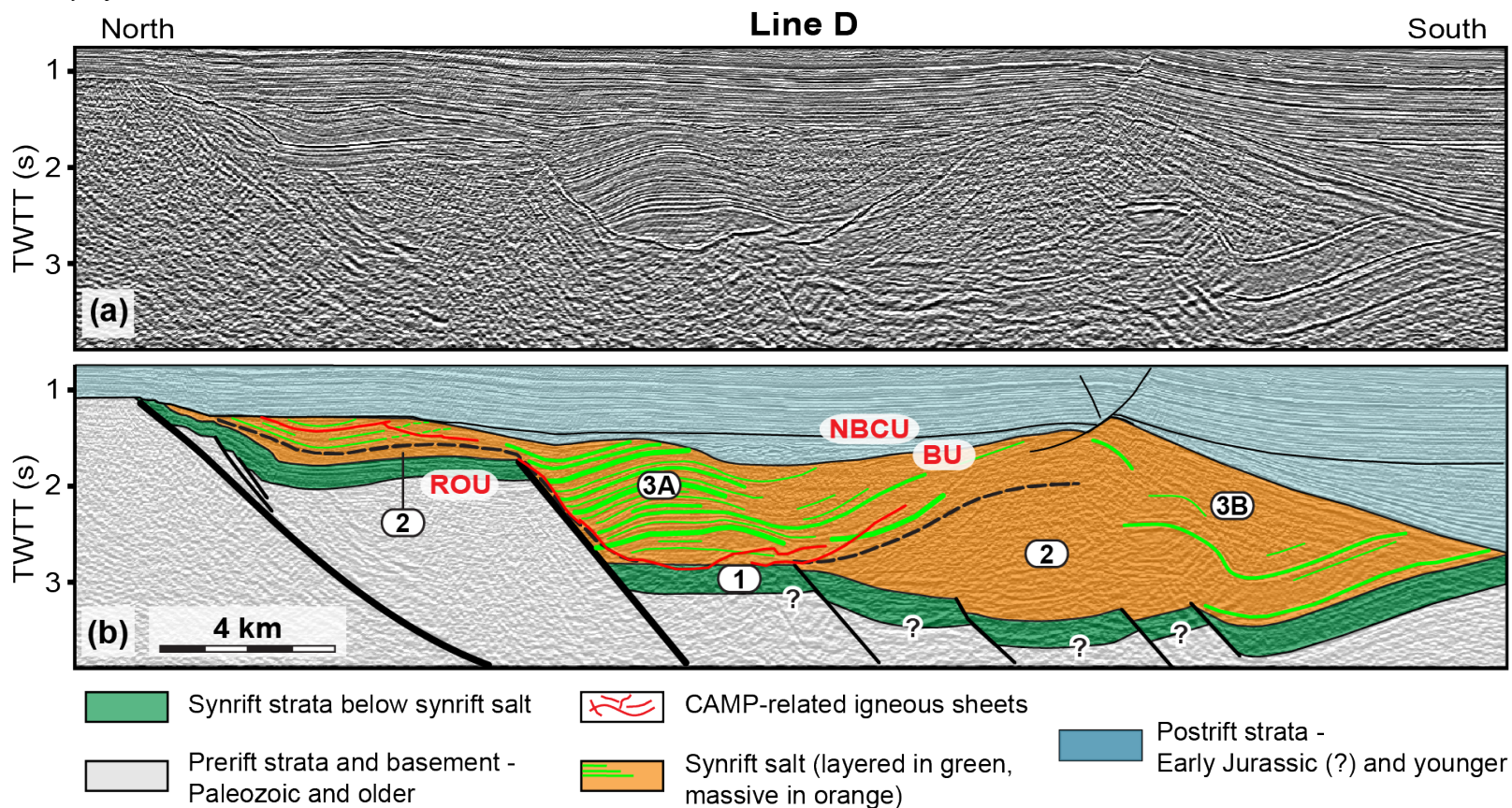
velocity of 4.5 km/s.

Figure 12. *Uninterpreted (**a**) and interpreted (**b**) versions of Line D (see Fig. 1b for location). Synrift package consists of four units: Unit 1 (synrift presalt), Unit 2 (lower part of synrift salt), Unit 3 (upper part of synrift salt), and Unit 4 (minibasin or synrift suprasalt). Facies 3A occurs near border-fault zone and facies 3B occurs far from border-fault zone. Facies 3A contains numerous internal seismic reflections, whereas Facies 3B contains fewer internal reflections. ROU: Rift-onset unconformity; BU: Breakup unconformity; NBCU: Near-base Cretaceous unconformity; CAMP: Central Atlantic Magmatic Province; TWTT: Two-way travel time. Dashed black line indicates approximate boundary between Units 2 and 3. Seismic line is displayed 1:1 assuming a velocity of 4.5 km/s.*

4.4. CAMP-related igneous activity in the eastern Orpheus rift basin

The synrift package of the Orpheus rift basin contains anomalous, high-amplitude reflections with distinctive characteristics (Figs. 5, 6b). Many of these high-amplitude reflections terminate abruptly within the synrift section (Figs. 6b, 6d, 12). Although commonly parallel to subparallel to bedding, many locally cut through bedding, climbing to higher stratigraphic levels (Fig. 6b). Some high-amplitude reflections are present along basement-involved faults (Figs. 10, 12), whereas others bifurcate or splay, forming a complex array of high-amplitude reflections (Fig. 12). Although no well has drilled these high-amplitude reflections in the Orpheus rift basin, their distinctive seismic and geometric characteristics are indicative of intrusive igneous sheets (e.g., Planke et al., 2005). Igneous sheets, having high densities (2.8 - 3.0 g/cm^3) and seismic velocities (5.5 - 6.5 km/s) compared to those of sedimentary rocks (Planke et al., 1999; Berndt et al., 2000; Planke et al., 2005), produce high-amplitude reflections on seismic profiles. Thus, based on the distinctive characteristics of the high-amplitude reflections in the eastern Orpheus rift basin, we conclude that they are likely associated with intrusive igneous sheets.

The high-amplitude reflections are present throughout the synrift package in the eastern Orpheus rift basin. As discussed previously, synrift deposition likely began by the Late Triassic and continued into the Early Jurassic (e.g., MacLean and Wade, 1992; Weston et al., 2012; Withjack et al., 2012; Sues and Olsen, 2015). Thus, the magmatic activity associated with the high-amplitude reflections must have occurred after the deposition of the synrift strata preserved in the basin (i.e., during or/and after the Late Triassic). Furthermore, the breakup unconformity truncates some high-amplitude events (Figs. 6b, 11). Because the breakup unconformity separates the synrift strata from the overlying late Middle Jurassic postrift strata (OETR, 2014), this magmatic activity must have occurred during and/or after the Late Triassic and during and/or

191 before the late Middle Jurassic. Based on this time interval as well as the numerous reports of

192 CAMP-related igneous rocks in the region surrounding the Orpheus rift basin (e.g., Dostal and

193 Greenough, 1992; McHone, 1992; Pe-Piper et al., 1992; Dostal and Durning, 1998; Cirilli et al.,

194 2009; Jourdan et al., 2009), we propose that these igneous sheets are likely associated with

195 CAMP, which as discussed previously, is a major igneous province that formed in latest Triassic

196 to earliest Jurassic time (McHone, 1992; Pe-Piper et al., 1992; Olsen et al., 2003; Marzoli et al.,

197 2011; Blackburn et al., 2013; Davies et al., 2017; Marzoli et al., 2018; Marzoli et al., 2019).

198

199 **5. DETAILED DESCRIPTION OF SYNRIFT UNITS IN THE EASTERN ORPHEUS**

200 **RIFT BASIN**

201 As mentioned previously, reflections within the synrift package have highly variable

202 geometries (Fig. 2). We have subdivided the synrift package into four separate units with

203 distinctive characteristics.

204

205 **5.1. Synrift Units 1-3**

206 Unit 1, the oldest, directly overlies the prerift strata (Fig. 5). In the study area, its maximum

207 thickness is ~0.4 second TWTT (~ 0.9 km). It consists of subparallel reflections that are gently

208 folded and offset by basement-involved intrabasin faults with normal separation. Locally,

209 internal reflections within Unit 1 thin toward the footwall of the border-fault system (Figs. 5, 6a,

210 12), reflecting gentle folding associated with movement on the border-fault system during

211 deposition. The exact cause of this folding is unclear, but it is likely fault-propagation folding

212 associated with the presence of Paleozoic prerift salt during basement-involved faulting (Gibling

213 et al., 2008).

214   Unit 2 overlies Unit 1, lacks internal seismic reflections, and has significant thickness

215   variations ranging from less than 0.1 s TWTT (~0.2 km) to ~1.5 s TWTT (~3.4 km) (Figs. 5, 12).

216   For example, on Line C (Fig. 5), Unit 2 thins northward, becoming thin or absent near the

217   border-fault system. Unit 2 also thickens within the cores of anticlines and thins beneath

218   synclines (Fig. 8). In some parts of the basin, Unit 2 mixes with the overlying Unit 3 forming

219   massive walls and columns (Fig. 10). Unit 2 commonly serves as a major detachment level

220   within the synrift package that decouples the deep and shallow deformation (Fig. 8), further

221   indicating a highly ductile behavior.

222   Unit 3 overlies Unit 2 and has two distinct interfingering seismic facies (i.e., 3A and 3B).

223   Facies 3A consists of numerous coherent and parallel-to-subparallel reflections, whereas Facies

224   3B is acoustically more transparent with few internal reflections (e.g., Fig. 5). Commonly, these

225   internal reflections are discontinuous, chaotic, and moderately to intensely folded (Fig. 10).

226   Multiple seismic lines in the study area show a systematic change of Unit 3 in both dip (N-S)

227   and strike (E-W) directions relative to the border-fault system. For example, on Lines C, B, and

228   D (Figs. 5, 8, 12), Unit 3 has numerous internal reflections in the north and becomes more

229   seismically transparent with fewer internal reflections in the south. Similarly, on Line G (Fig.

230   13), the number of coherent internal reflections in Unit 3 decreases toward the west within a

231   structural high (Fig. 9a), further corroborating the lateral variability within Unit 3. These two

232   facies have distinctly different deformational styles. Shortening-related structures such as

233   detached folds and thrust faults are common in Facies 3A (Figs. 6a, 7d, 8), whereas Facies 3B,

234   where deformed, forms large walls and columns and exhibits highly ductile behavior (Figs. 7g,

235   10). The parallel internal reflections in Unit 3 show that its deposition was widespread in a

236   broad, subsiding basin and that most deformation occurred after deposition. Locally, growth
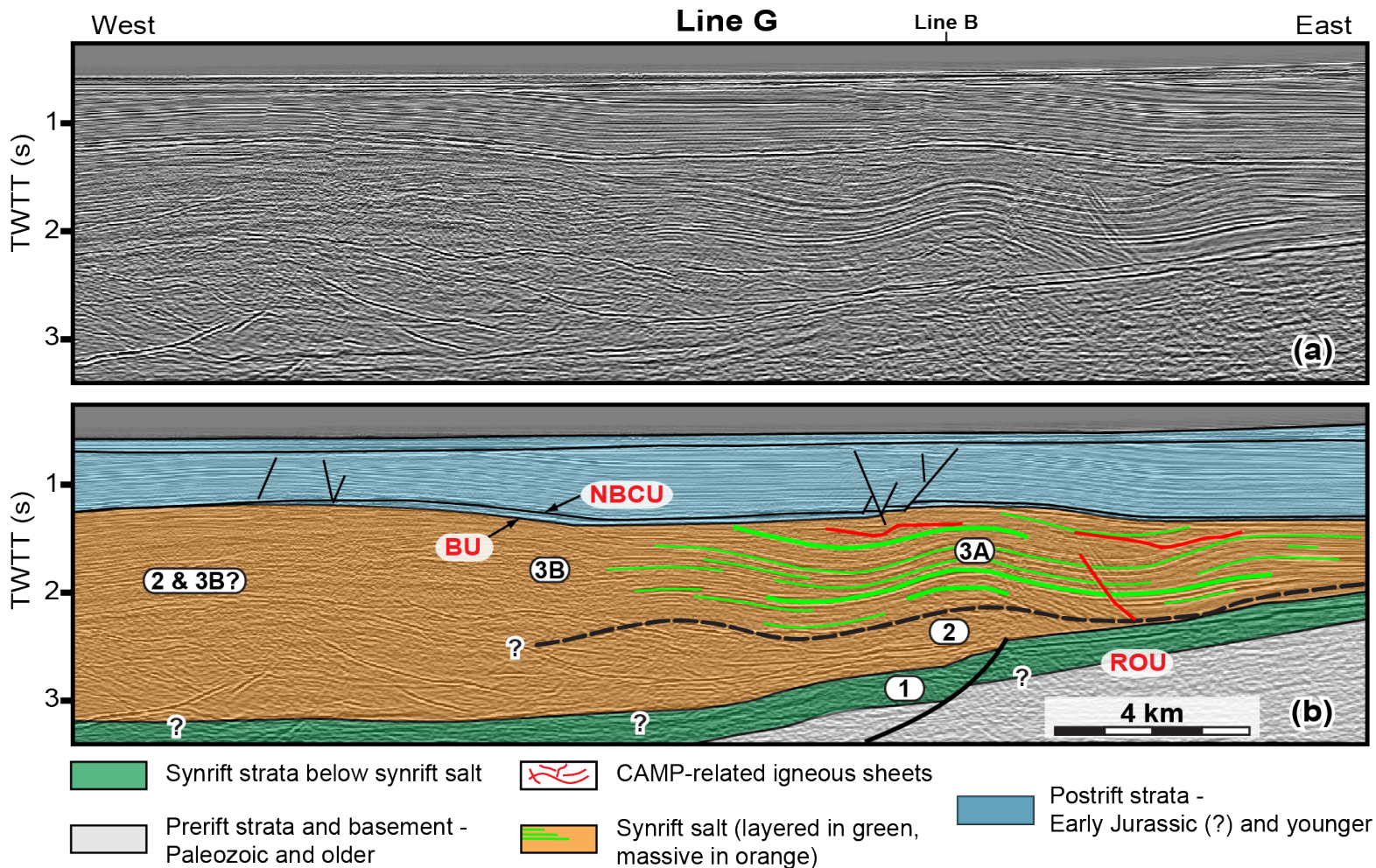
Figure 13. *Uninterpreted (**a**) and interpreted (**b**) versions of Line G (see Fig. 1b for location). Synrift package consists of four units: Unit 1 (synrift presalt), Unit 2 (lower part of synrift salt), Unit 3 (upper part of synrift salt), and Unit 4 (minibasin or synrift suprasalt). Note facies change in Unit 3 along strike of basin (i.e., west-east). Facies 3A contains numerous internal seismic reflections, whereas Facies 3B contains fewer internal reflections. ROU: Rift-onset unconformity; BU: Breakup unconformity; NBCU: Near-base Cretaceous unconformity; CAMP: Central Atlantic Magmatic Province; TWTT: Two-way travel time. Dashed black line indicates approximate boundary between Units 2 and 3. Seismic line is displayed 1:1 assuming a velocity of 4.5 km/s.*

244 strata of Facies 3A are associated with fault-propagation folds adjacent to and above the northern

245 border-fault segments (Figs. 5, 6b). Here, the internal reflections of Facies 3A converge and thin

246 toward the footwall of the border-fault system, indicating that the border-fault system was active

247 during the deposition of Unit 3.

248

249 **5.2. Unit 4**

250   Unit 4 is the synrift component of the fill within asymmetric synclines in the hanging-wall

251 of the border-fault system (Figs. 6d, 8, 10). Most internal reflections within Unit 4 either thin or

252 thicken toward the adjacent wall or columns (Fig. 10) or detachment folds (Fig. 8). In the study

253 area, the vertical thickness of Unit 4 can reach up to 2.5 second TWTT (~5.6 km).

254

255 **6. INTERPRETATION OF THE SYNRIFT UNITS IN THE EASTERN ORPHEUS RIFT**

256   **BASIN**

257 **6.1. Lithologies and ages of synrift units 1 to 3**

258   Unit 1, the oldest synrift unit in the Orpheus rift basin, is gently folded and cut by basement-

259 involved faults (i.e., it has a brittle behavior), whereas overlying Unit 2 exhibits a highly ductile

260 behavior, acting as a major detachment level and having significant thickness variations. The

261 overlying Unit 3 has two coeval facies, each with distinct characteristics and behaviors. Facies

262 3A has pronounced internal layering that is folded and faulted, whereas Facies 3B lacks

263 significant internal layering and commonly exhibits a highly ductile behavior. Facies 3B,

264 together with the underlying Unit 2, commonly mix to produce large walls and columns in the

265 study area.

266   No wells have penetrated these units in the study area, and the intense deformation within

267   the synrift package, particularly Units 2 and 3, prevents a direct seismic correlation with the

268   available well data from the western part of the basin. However, we can infer the lithology of

269   these units based on their seismic characteristics, their mechanical behaviors, and geologic

270   information from the ENAM rift basins that surround the eastern Orpheus rift basin. We interpret

271   Unit 1, with its brittle behavior and deep stratigraphic location, as part of the Eurydice

272   Formation, the oldest synrift formation in the region (Wade and MacLean, 1990; MacLean and

273   Wade, 1992, 1993; Tanner and Brown, 2003) (Fig. 14). Well data from the western Orpheus rift

274   basin and surrounding rift basins suggest that the Eurydice Formation likely consists of clastic

275   sedimentary rocks. We interpret Units 2 and 3, with their ductile behavior and their stratigraphic

276   location above Unit 1, as part of the synrift salt of the Argo Formation (Fig. 14). Unit 2, lacking

277   internal reflections, likely consists of massive salt, whereas Unit 3, with internal reflections,

278   consists of salt with variable amounts of interbedded sedimentary layers. Interbedded

279   sedimentary layers in other salt basins include other evaporites (i.e., gypsum, anhydrite),

280   carbonates, shales, siltstones, or igneous rocks (Van Gent et al., 2011; Jackson et al., 2015;

281   Rowan et al., 2019). Well data from the western Orpheus rift basin and the surrounding ENAM

282   rift basins indicate that salt of the Argo Formation is interbedded mainly with shale (Holser et

283   al., 1988; Wade and MacLean, 1990; MacLean and Wade, 1992, 1993; Weston et al., 2012) (Fig.

284   3). Therefore, we propose that Facies 3A and 3B of Unit 3 are shale-rich and shale-poor salt

285   facies, respectively, of the Argo Formation. Thus, the thick synrift package in the eastern

286   Orpheus rift basin, with the exception of a thin unit of Eurydice Formation as its base, is

287   composed primarily of massive and interbedded rock salt of the Argo Formation.
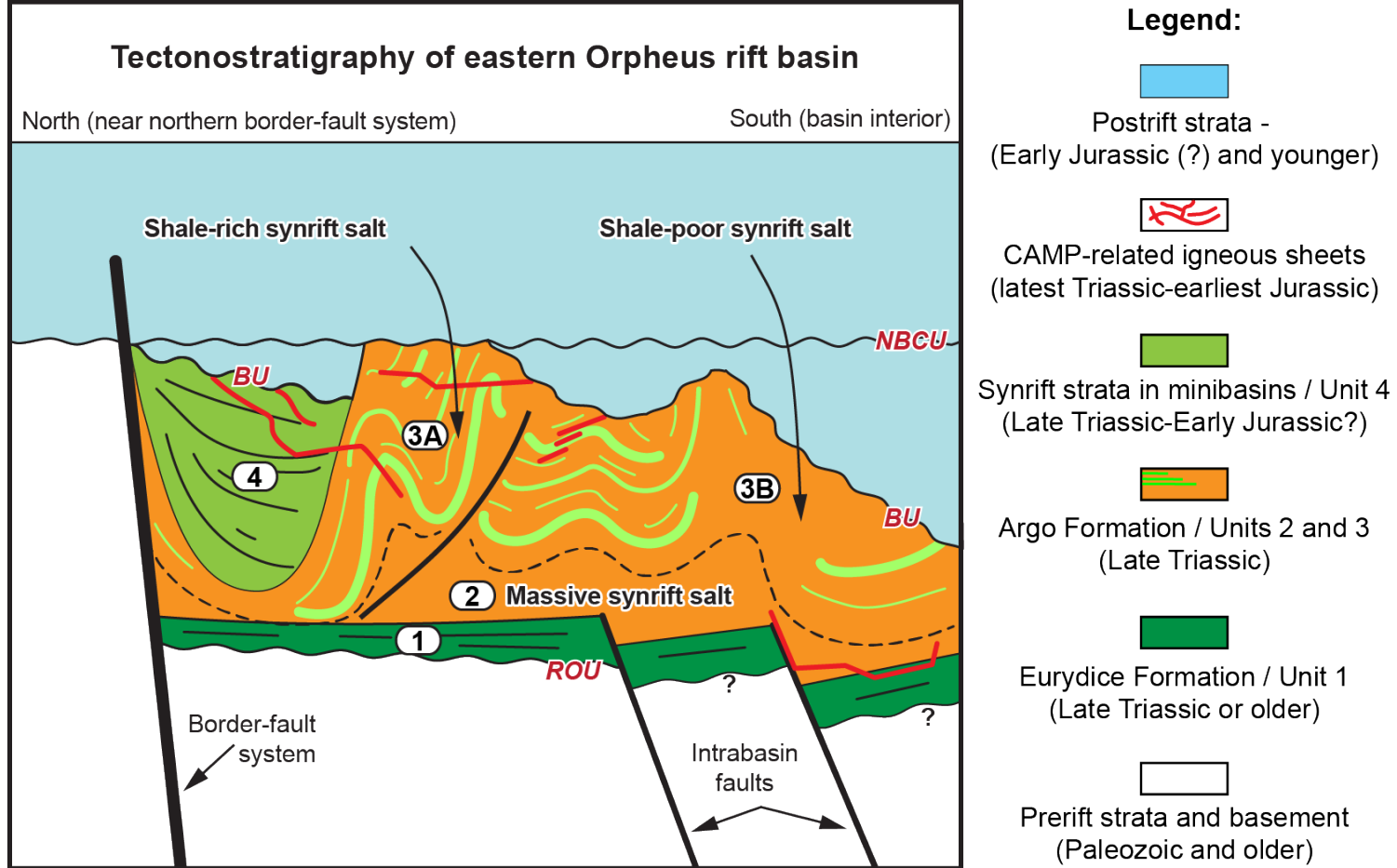
Figure 14. *Vertically exaggerated (2x), schematic cross section showing proposed tectonostratigraphy of the eastern Orpheus rift basin. Note that the synrift Argo Formation varies temporally (i.e., Units 2 and 3) and laterally (i.e., Facies 3A and 3B), and that CAMP-related igneous sheets are present within the eastern Orpheus rift basin, intruding all synrift units. Dashed black line indicates approximate boundary between Units 2 and 3. CAMP: Central Atlantic Magmatic Province; NBCU: Near-base Cretaceous unconformity; BU: Breakup unconformity; ROU: Rift-onset unconformity.*

294   Using well data from the western Orpheus rift basin, Bujak and Williams (1977) and Barss

295   et al. (1979) determined the palynological age of the Argo Formation as Early Jurassic (i.e.,

296   Hettangian-Sinemurian). As explained below, this palynological age is not consistent with our

297   seismic observations from the eastern Orpheus rift basin. CAMP was a short-lived magmatic

298   event (< 1 my) that began during the latest Triassic and ended during the earliest Jurassic (see

299   Section 2). As discussed previously, igneous sheets, likely related to CAMP, intrude the entire

300   synrift package in the eastern Orpheus rift basin (e.g., Figs. 11, 12). If these are CAMP-related

301   igneous sheets, then the deposition of the preserved synrift section in the eastern Orpheus rift

302   basin would predate the CAMP-related igneous activity, and the thick salt-rich section in the

303   eastern Orpheus rift basin (Units 2 and 3) would have a Late Triassic age (Fig. 14). Thus, the

304   salt-rich section in the eastern Orpheus rift basin would be equivalent to the Late Triassic salt

305   encountered in the ENAM rift basins that surround the Orpheus rift basin, including the Mohican

306   rift basin (Scotian Shelf) to the south (Weston et al., 2012) and the Grand Banks rift basins to the

307   north (Holser et al., 1988) and would be older than the Early Jurassic salt observed in the

308   western Orpheus rift basin.

309   The presence of the Late Triassic salt in our study area would indicate that deposition of

310   synrift salt likely began in the eastern Orpheus rift basin in the Late Triassic and expanded to the

311   west by Early Jurassic time. Erosion after rifting associated with the formation of the breakup

312   unconformity (BU) may have removed any Early Jurassic synrift salt from the study area. If the

313   Argo Formation (i.e., Units 2 and 3) in the eastern Orpheus rift basin is Late Triassic in age, then

314   underlying Unit 1, representing the Eurydice Formation, is Late Triassic or older (Fig. 14).

315

316   **6.2. Deposition, composition, and age of Unit 4**

317   Unit 4, the youngest unit, accumulated within asymmetric synclines near the northern

318   border-fault system. The growth strata within Unit 4 generally thin or thicken toward and/or

319   onlap onto adjacent salt walls and columns composed of Units 2 and 3 of the Argo Formation,

320   indicating that Unit 4 was deposited during salt flow. This also suggests that sedimentary loading

321   associated with the deposition of Unit 4 promoted lateral salt flow from beneath the synclines to

322   the adjacent growing salt structures. Thus, these synclines are similar to the salt withdrawal

323   minibasins (Hudec et al., 2006; Goteti et al., 2012; Rowan, 2019) commonly observed in other

324   salt provinces (e.g., Diegel et al., 1995; Callot et al., 2014; Saura et al., 2014; Jackson et al.,

325   2015; Martin-Martin et al., 2017; Teixell et al., 2017). No wells have penetrated the minibasins

326   in the eastern Orpheus rift basin, making it difficult to interpret the lithology of the minibasin fill.

327   Because the minibasins in our study area developed exclusively near the northern border-fault

328   system, Unit 4 may consist, at least in part, of coarse-grained and poorly sorted, alluvial-fan

329   deposits as commonly observed adjacent to the border faults of other rift basins (e.g., Gawthorpe

330   et al., 1990; Leeder and Jackson, 1993; Gupta et al., 1999; Allen and Heller, 2012; Ford et al.,

331   2013) or rock-fall deposits associated with nearby fault talus, similar to that observed in the

332   adjacent Fundy rift basin (Olsen and Schlische, 1990; Tanner and Hubert, 1991; Withjack et al.,

333   2009; Withjack et al., 2010).

334   Despite limited information about these minibasins, we propose that sedimentary rocks of

335   Unit 4 are likely synrift rocks of latest Triassic to Early Jurassic age (Fig. 14). Unit 4

336   stratigraphically overlies the synrift salt of Unit 3 and is intruded by likely CAMP-related

337   igneous sheets (Figs. 6d, 11), indicating that its deposition would have begun after the deposition

338   of the Late Triassic salt and before and/or during CAMP-related magmatic activity in the latest

339   Triassic to earliest Jurassic. The formation of some minibasins may have continued after CAMP-

340 related activity until the breakup in the Early Jurassic. Identification of the breakup unconformity

341 throughout the region (based on loop ties with areas where synrift and postrift strata are clearly

342 distinguishable) indicates that the development of some minibasins resumed after the formation

343 of the breakup unconformity (e.g., Figs. 10, 11). The age of the postrift strata in the minibasins is

344 unclear, but they likely represent the oldest postrift rocks in the region (i.e., Middle Jurassic or

345 older) (OETR, 2014).

346

347 **6.3. Origin and timing of detached shortening**

348   As previously described, shortening-related structures such as detachment folds and thrust

349 faults are common in the shale-rich salt facies of Unit 3 (i.e., Facies 3A). Because the folded

350 strata have a relatively constant thickness (i.e., lack growth beds associated with the

351 folding/faulting) and are truncated by the breakup unconformity, most of the detached shortening

352 occurred after the deposition of Unit 3 and before/during the formation of the breakup

353 unconformity. The minibasins near the northern border faults contain the youngest synrift unit

354 that accumulated after deposition of the synrift salt. Growth strata in the minibasins thin and

355 onlap onto the salt bodies containing the shortening-related structures, indicating that the

356 formation of these structures and minibasins was synchronous. Based on these observations, we

357 propose that detached shortening caused by lateral salt flow during the subsidence of the

358 minibasins produced most of the detached, shortening-related structures (Fig. 17). This is

359 consistent with experimental studies that show that sediment loading above a salt layer (Ge et al.,

360 1997a; Ge et al., 1997b; Hudec et al., 2006; Hudec and Jackson, 2011) could cause the salt to

361 move laterally, leading to the formation of shortening-related structures (Rowan et al., 2004).

362   The presence of CAMP-related igneous sheets is critical to constrain the timing of

363   shortening. As discussed above, the growth strata in Unit 4 indicate that most shortening was

364   coeval with minibasin formation. In our study area, likely CAMP-related igneous rocks intruded

365   both the folded strata of shale-rich salt unit (Unit 3, Figs. 8, 12) and the minibasins (Unit 4, Figs.

366   6d, 11). Based on this observation, we propose that significant amount of detached shortening

367   and the coeval minibasin formation began before CAMP-related igneous activity. Specifically,

368   because CAMP activity occurred at ~201 Ma (Marzoli et al., 2011; Blackburn et al., 2013;

369   Davies et al., 2017; Marzoli et al., 2019), most detached shortening began before the latest

370   Triassic. Furthermore, because some minibasins contain both synrift and postrift strata (e.g.,

371   Figs. 10, 11), some detached shortening and salt diapirism continued during and after CAMP

372   activity and resumed during and/or after the formation of the breakup unconformity in the Early

373   to Middle Jurassic.

374   The cause and timing of some shortening-related structures in the southern part of the basin,

375   however, remain enigmatic. For example, some steeply dipping and folded strata of Facies 3A

376   are present far south of the minibasins (e.g., Fig. 8), indicating that these structures may have an

377   origin unrelated to minibasin formation. Because these folded strata are present above a major

378   basement-involved, intrabasin fault and truncated by the overlying breakup unconformity, the

379   structures may have resulted from the reactivation of the fault with left-lateral and reverse

380   components of slip during the rift-drift transition as proposed for faults in the adjacent Fundy rift

381   basin (Baum et al., 2008; Withjack et al., 2009; Withjack et al., 2010).

382

383   **7.   DISCUSSION**

384   **7.1. Factors that influence deformation style in salt-rich rift basins**

385   Structures vary considerably throughout the eastern Orpheus rift basin, ranging from

386   basement-involved faults, to fault-propagation folds above basement-involved faults, to

387   detachment folds and detached thrust faults, to intensely folded intrasalt stringers within massive

388   salt walls and columns (Fig. 7). We propose that two factors profoundly impacted the

389   deformational style of the eastern Orpheus rift basin and, by analogy, other salt-rich rift basins:

390   1) the basement-involved border-fault system, and 2) the mechanical stratigraphy of the synrift

391   salt (i.e., massive vs. interbedded).

392

393   **7.1.1.   Arrangement and activity of basement-involved border-fault system**

394   Rifting produced an E-striking border-fault system in the northern part of the eastern

395   Orpheus rift basin. The shale-rich salt facies of Unit 3 (i.e., Facies 3A) is most prevalent in the

396   northern part of the basin near the border-fault system and its relay ramps, whereas the shale-

397   poor salt of Facies 3B developed farther from the border-fault system (Fig. 9c). This relationship

398   suggests that the relay ramps of the border-fault system connected the footwall region outside of

399   the basin with the hanging-wall basin interior, providing pathways for clastic sediments to enter

400   the basin and promoting the deposition of interbedded salt and shale (Fig. 15). Reports from

401   other rift basins and modeling results suggest that ramp-parallel channel systems may deliver

402   these clastic sediments into the hanging wall region during rifting, allowing them to accumulate

403   at the base of the relay ramps (Athmer et al., 2010; Athmer and Luthi, 2011; Hopkins and

404   Dawers, 2018).

405   The sediments of the youngest synrift unit (Unit 4) accumulated within minibasins in the

406   hanging wall directly adjacent to the border-fault system, suggesting an increased sediment

407   influx into the basin from the adjacent footwall region during the later stages of rifting. The high

408   level of sedimentation likely reflects the development of footwall drainage systems that eroded

409   the footwall rocks and delivered clastic sediments directly into the hanging walls of the border

410   faults (Gawthorpe and Leeder, 2000; Densmore et al., 2004; Elliott et al., 2012). The deposition

411   of these sedimentary rocks is important in producing a differential load above the salt (Hudec et

412   al., 2006; Rowan, 2019), creating lateral salt flow toward the south, and eventually triggering

413   detached deformation in the eastern Orpheus rift basin.
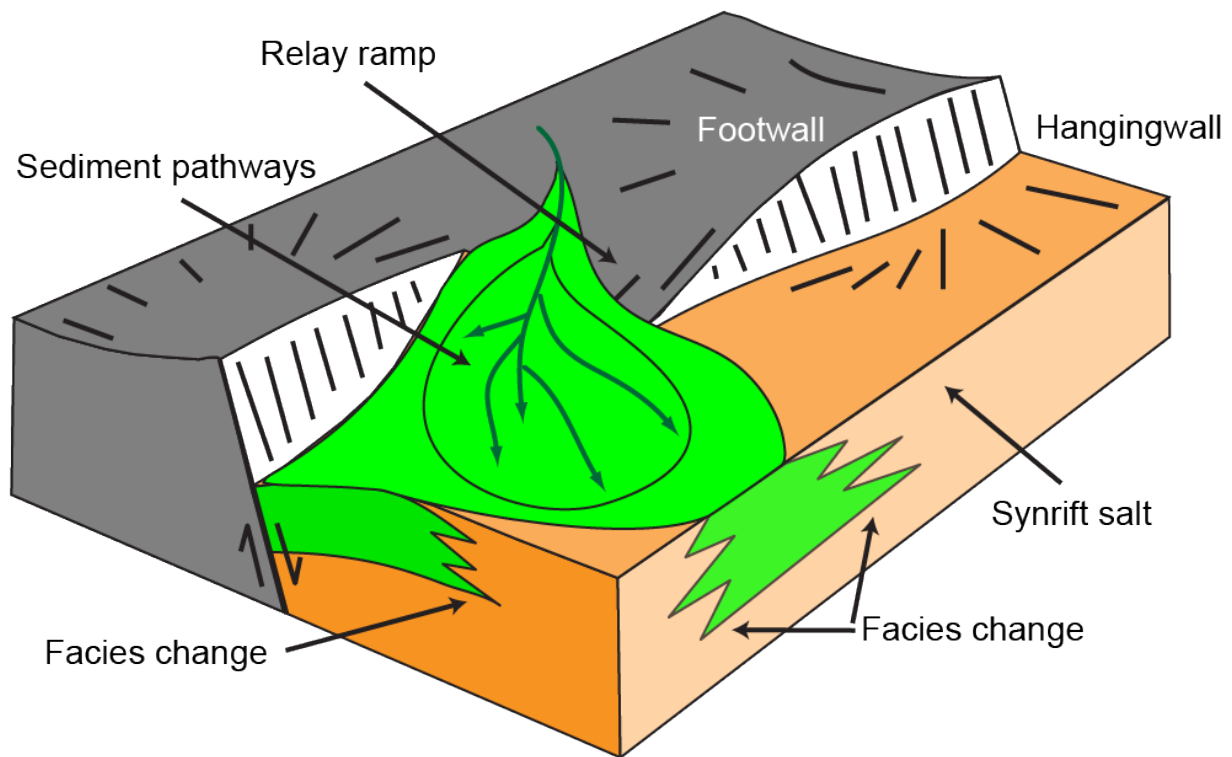
414

415   *Figure 15. Schematic diagram showing relay ramp influencing facies distribution of synrift salt*
416   *in rift basins (modified from Withjack et al., 2002). Relay ramp connected footwall with basin*
417   *depocenter, providing pathways for clastic sediments to enter the basin.*

418

419   **7.1.2. Mechanical stratigraphy of synrift salt**

420   The presence of interbedded shales strongly influenced the bulk behavior of the synrift salt

421   of the Argo Formation, which ultimately controlled the deformation style of the eastern Orpheus

422   rift basin (Fig. 16). Detachment folds and thrust faults affected Facies 3A with its abundant

423   interbedded shales and accommodated the shortening associated with lateral salt movement

424   during minibasin formation (Fig. 16). In contrast, Facies 3B with few interbedded shales

425   exhibited a highly ductile behavior, combining with Unit 2 to form massive salt walls and

426   columns adjacent to the minibasins (Fig. 16). These walls and columns had complex internal

427   deformation with tightly folded and faulted intrasalt stringers.
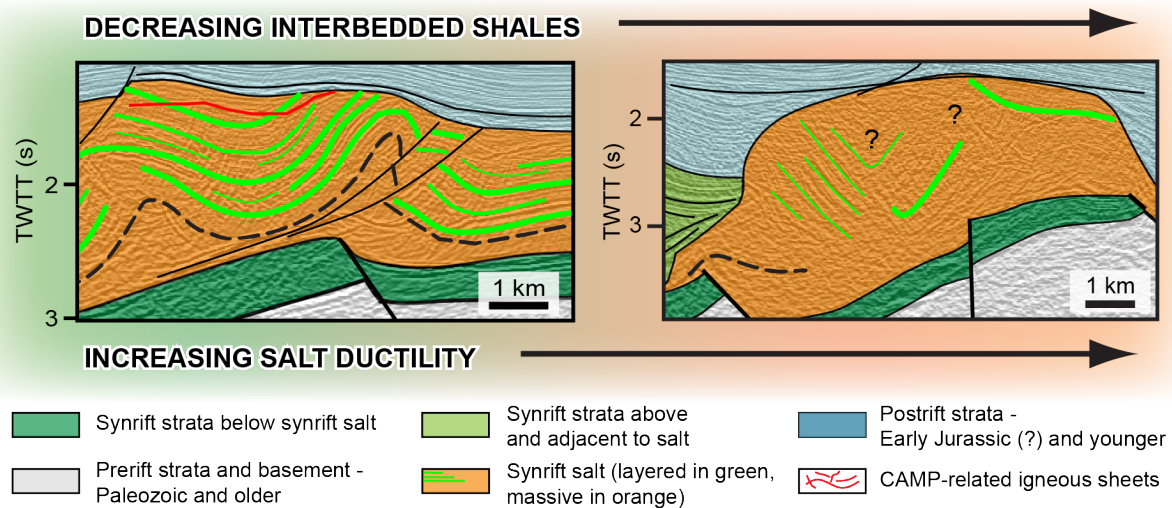
428

429   *Figure 16. Parts of Line B (left) and Line F (right) summarizing effects of interbedded*

430   *sedimentary layers within salt on deformation patterns. The presence of abundant interbedded*

431   *sedimentary layers reduces the ductility of the salt. Seismic lines are displayed 1:1 assuming a*

432   *velocity of 4.5 km/s. Dashed black line indicates approximate boundary between lower massive*

433   *salt and upper salt containing interbedded shales. CAMP: Central Atlantic Magmatic Province;*

434   *TWTT: Two-way travel time.*

435

436   The contrasting behaviors of the massive salt in Unit 2 and the interbedded salt and shale in

437   Facies 3A also promoted the formation of fault-propagation folds in the shallow synrift strata

438   (Figs. 5, 6b). Specifically, the lower massive salt of Unit 2 with its highly ductile behavior

439   decoupled the deep and shallow deformation. As a result, broad fault-propagation folds

440   developed within Facies 3A to accommodate the displacement on the underlying basement-
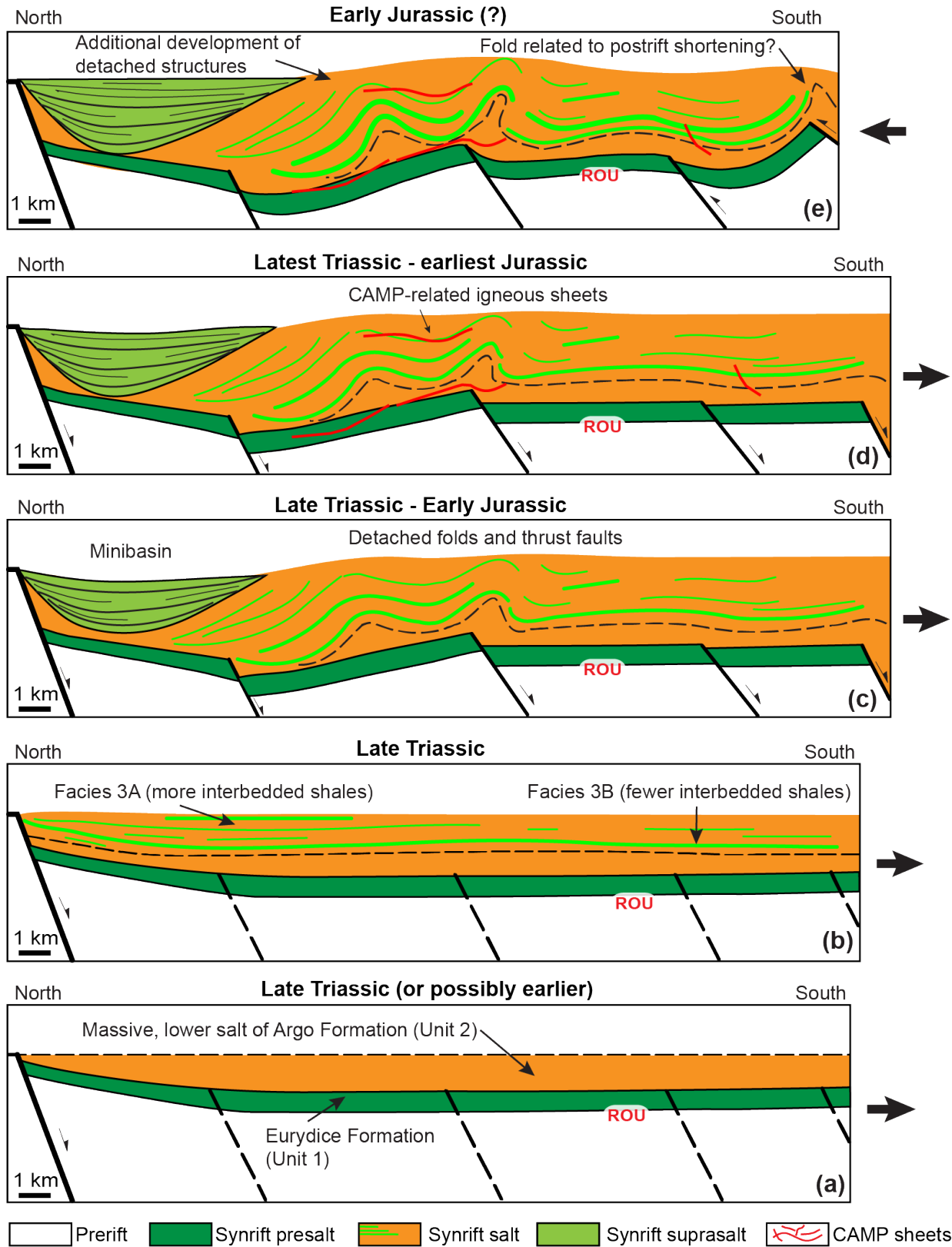
441   involved faults. Our interpretation is consistent with the results of scaled experimental models

442   that show the presence of salt can decouple the deep and shallow deformation and facilitate the

443   formation of fault-propagation folds above a normal fault (Withjack and Callaway, 2000).

444

445   **7.2. The structural evolution of the eastern Orpheus basin during and immediately after**

446   **rifting**

447   During the early stages of rifting in the Late Triassic (or possibly earlier), the E-striking, S-

448   dipping border-fault system of the eastern Orpheus rift basin began to form, allowing Unit 1 (i.e.,

449   the Eurydice Formation) and overlying Unit 2 (i.e., the massive salt of the lower Argo

450   Formation) to accumulate within a wide rift basin (Fig. 17a). As rifting continued, major relay

451   ramps developed within the border-fault system, influencing depositional patterns during the

452   accumulation of the upper Argo Formation (Unit 3) (Fig. 17b). The amount of interbedded shale

453   within the upper Argo Formation varied laterally, depending on proximity to the relay ramps

454   (Fig. 17b). Facies 3A with many interbedded shale layers formed within and near the relay

455   ramps, whereas Facies 3B with few interbedded shale layers formed far from the relay ramps.

456   During the later stages of rifting (Late Triassic), new basement-involved, intrabasin faults

457   formed south of the border-fault system (Fig. 17c). Many of these intrabasin faults dip to the

458   south and offset the Eurydice Formation (Unit 1) with normal separation. Movement on these

459   subsalt faults resulted in the development of broad monoclines (i.e., fault-propagation folds)

460   within the overlying synrift strata. Additionally, minibasins developed adjacent to the border-

461   fault system with deposition of alluvial fans and/or the accumulation of talus-slope deposits in

462   the hanging wall. As the minibasins developed, sedimentary loading forced the underlying salt to

463   move laterally toward the south, producing detachment folds, detached thrust faults, and salt

Early Jurassic (?)

North

South

Additional development of detached structures

Fold related to postrift shortening?

ROU

1 km

(e)

Latest Triassic - earliest Jurassic

North

South

CAMP-related igneous sheets

ROU

1 km

(d)

Late Triassic - Early Jurassic

North

South

Minibasin

Detached folds and thrust faults

ROU

1 km

(c)

Late Triassic

North

South

Facies 3A (more interbedded shales)

Facies 3B (fewer interbedded shales)

ROU

1 km

(b)

Late Triassic (or possibly earlier)

North

South

Massive, lower salt of Argo Formation (Unit 2)

Eurydice Formation (Unit 1)

ROU

1 km

(a)

Prerift   Synrift presalt   Synrift salt   Synrift suprasalt   CAMP sheets

464

42

Figure 17. Schematic restoration of Line B (see Fig. 1b for location), showing eastern Orpheus basin development during Late Triassic (or possibly earlier) to Early Jurassic. *(a)* During early rifting, the deposition of clastic sediments (Eurydice Formation, Unit 1) preceded deposition of massive salt of the Argo Formation (Unit 2). Note that basement-involved faulting was focused on the northern border-fault system, producing a wide basin with widespread deposition. *(b)* As rifting progressed, the development of relay ramps on the border-fault system promoted the input of clastic sediments into the basin. This resulted in lateral variability of the Argo salt with interbedded salt near the relay ramps (Facies 3A) and more massive salt far from the relay ramps (Facies 3B). *(c)* Activity continued on the border-fault system and basement-involved, intrabasin faults developed. Also, minibasins (likely associated with differential sediment loading near the border-fault system) caused salt to move laterally, producing detached shortening. *(d)* CAMP-related igneous sheets intruded the synrift strata. *(e)* Some basement-involved faults may have been reactivated with left-lateral and reverse components of slip during the rift-drift transition, leading to additional development of shortening-related structures. ROU: Rift-onset unconformity; CAMP: Central Atlantic Magmatic Province. Black dashed line indicates approximate boundary between lower massive salt and upper salt containing interbedded shales.

walls/columns (Fig. 17c). In latest Triassic/earliest Jurassic time, widespread igneous activity associated with the Central Atlantic Magmatic Province (CAMP) affected the eastern Orpheus rift basin (Fig. 17d) with numerous igneous sheets intruding the entire synrift section (Units 1-4). During the transition from rifting to drifting in the Early Jurassic, some of the basement-involved faults may have been reactivated with left-lateral and reverse components of slip, producing the steeply dipping strata and tight folds directly above basement-involved faults in the southern part of the basin far from the border-fault system and minibasins (Figs. 8, 17e).

8. CONCLUSIONS

1. The eastern Orpheus rift basin exhibits an array of basement-involved and detached structures. The basement-involved structures include the northern border-fault system and the intrabasin faults, all of which have normal separation. The detached structures

494   developed above the basement-involved fault blocks, and range from fault-propagation

495   folds, to detachment folds and thrust faults, to salt diapirs.

496 2. The eastern Orpheus rift basin and overlying Scotian postrift basin have three angular-

497   unconformity-bound tectonostratigraphic packages: prerift, synrift, and postrift. The

498   prerift package represents Paleozoic and crystalline basement, whereas the postrift

499   package represents Middle Jurassic and younger strata. The rift-onset unconformity

500   (ROU) separates the prerift from the overlying synrift strata, whereas the breakup

501   unconformity (BU) and near-base Cretaceous unconformity (NBCU) define the top of the

502   synrift package in the north and south of our study area, respectively.

503 3. The synrift package of the eastern Orpheus rift basin has four distinct units. Unit 1, the

504   oldest, likely represents the clastic sedimentary rocks of the Eurydice Formation, whereas

505   Units 2 and 3 together likely represent synrift salt of the Argo Formation. Unit 2 is

506   massive, whereas the overlying Unit 3 has two interfingering facies. Facies 3A consists

507   of interbedded salt and shales and Facies 3B is mostly massive salt with few interbedded

508   shale layers. Unit 4, the youngest synrift unit, accumulated exclusively within minibasins

509   near the border-fault system. The lithology of Unit 4 is unclear. Its proximity to the

510   northern border-fault system, however, suggests that it might consist, at least in part, of

511   coarse-grained and poorly sorted alluvial-fan or talus-slope deposits.

512 4. All of the synrift strata in the eastern Orpheus rift basin are intruded by igneous sheets

513   likely associated with the Central Atlantic Magmatic Province (CAMP) that developed

514   during the latest Triassic to earliest Jurassic. If so, the synrift units in the eastern Orpheus

515   rift basin are mostly Late Triassic in age, and the synrift salt in the eastern Orpheus rift

516   basin is older than that encountered in wells from the western part of the basin,

517   suggesting that deposition of synrift salt began in the eastern Orpheus rift basin in the

518   Late Triassic and expanded to the west by Early Jurassic time.

519   5. The eastern Orpheus rift basin underwent several major episodes of deformation

520   involving basement-involved and detached deformation during and immediately after

521   rifting: 1) the development of the northern border-fault system during the early stages of

522   rifting, 2) continued activity on the border-fault system, the development of intrabasin

523   basement-involved faults, and the coeval development of minibasins, detached

524   shortening-related structures, and salt diapirs, and 3) erosion, formation of the breakup

525   unconformity, and possible reactivation of some basement-involved faults with left-

526   lateral and reverse components of slip during the transition from rifting to drifting.

527   6. Two primary factors influenced the style of deformation in the eastern Orpheus rift basin

528   during and after rifting: 1) the arrangement and activity of the basement-involved border

529   faults, and 2) the mechanical stratigraphy of the synrift salt. Relay ramps of the border-

530   fault system provided pathways for clastic sediments to enter the salt-rich rift basin. As a

531   result, the sedimentation patterns of the synrift Argo Formation (i.e., Unit 3) varied from

532   interbedded salt and shales (Facies 3A) near the relay ramps to predominantly rock salt

533   (Facies 3B) in the middle of the basin. Subsequent minibasin development near the

534   border-fault system caused the underlying salt to flow laterally to the south, producing

535   salt walls and/or columns and detached shortening-related structures. The proportion of

536   salt-to-shale controlled the bulk deformation behavior of the synrift Argo Formation. The

537   shale-rich Facies 3A of the Argo Formation accommodated the shortening associated

538   with the lateral salt flow during minibasin formation by developing detached folds and

539   thrust faults. In contrast, the shale-poor Facies 3B of the Argo Formation had a highly

540   ductile behavior, and, together with Unit 2, formed salt walls and columns.

541

542   **9. ACKNOWLEDGMENTS**

543   We would like to thank our colleague, Zulfitriadi Syamsir, for his many valuable geologic

544   and geophysical contributions and insights during this study. We thank TGS, ConocoPhillips, the

545   Canadian Department of Natural resources, the Canada-Nova Scotia Offshore Petroleum Board

546   (CNSOPB), and Suncor Energy for providing the 2D seismic-reflection data used in this study.

547   We acknowledge the generosity of Schlumberger for providing Petrel, the software tool used to

548   interpret the seismic data. We also thank Husky Energy for providing general support of the

549   Rutgers Structure Group. Finally, we thank Rutgers University for providing support during this

550   study.

551

552   **10. REFERENCES**

553   Ainsworth, N. R., Riley, L. A., Bailey, H. W., Coles, G. P., & Gueinn, K. J. (2016). Jurassic-Tertiary
554   Stratigraphy of the Southern Newfoundland Margin - Wells: East Wolverine G-37, Eider
555   M-75, Emerillon M-75 & Narwhal F-99. *Riley Geoscience Limited. Report prepared for*
556   *Nalcor Energy.*
557   Allen, P. A., & Heller, P. L. (2012). Dispersal and Preservation of Tectonically Generated Alluvial
558   Gravels in Sedimentary Basins. In C. Busby & A. Azor (Eds.), *Tectonics of Sedimentary*
559   *Basins* (pp. 111-130).
560   Ascoli, P. (1988). Mesozoic-Cenozoic foraminiferal, ostracod and calpionellid zonation of the
561   North Atlantic margin of North America: Georges Bank-Scotian basins and northeastern
562   Grand Banks (Jeanne d'Arc, Carson and Flemish Pass basins). Biostratigraphic correlation
563   of 51 wells. *Geological Survey of Canada, Open File #1791*, 41.
564   Athmer, W., Groenenberg, R. M., Luthi, S. M., Donselaar, M. E., Sokoutis, D., & Willingshofer, E.
565   (2010). Relay ramps as pathways for turbidity currents: a study combining analogue
566   sandbox experiments and numerical flow simulations. *Sedimentology, 57*(3), 806-823.
567   doi:10.1111/j.1365-3091.2009.01120.x
568   Athmer, W., & Luthi, S. M. (2011). The effect of relay ramps on sediment routes and deposition:
569   A review. *Sedimentary Geology, 242*(1-4), 1-17. doi:10.1016/j.sedgeo.2011.10.002
570   Barss, M. S., Bujak, J. P., & Williams, G. L. (1979). Palynological zonation and correlation of sixty-
571   seven wells, eastern Canada. *Geological Survey of Canada, Paper 78-24*.

572　Baum, M. S., Withjack, M. O., & Schlische, R. W. (2008). *The Ins and Outs of Buttress Folds:*
573　　　　*Examples from the Inverted Fundy Rift Basin, Nova Scotia and New Brunswick, Canada*.
574　　　　Paper presented at the Central Atlantic Conjugate Margins Conference, Halifax.
575　Berndt, C., Skogly, O. P., Planke, S., Eldholm, O., & Mjelde, R. (2000). High-velocity breakup-
576　　　　related sills in the Vøring Basin, off Norway. *Journal of Geophysical Research: Solid*
577　　　　*Earth, 105*(B12), 28443-28454. doi:10.1029/2000jb900217
578　Blackburn, T. J., Olsen, P. E., Bowring, S. A., McLean, N. M., Kent, D. V., Puffer, J., McHone, G.,
579　　　　Rasbury, E. T., & Et-Touhami, M. (2013). Zircon U-Pb Geochronology Links the End-
580　　　　Triassic Extinction with the Central Atlantic Magmatic Province. *Science, 340*(6135), 941-
581　　　　945. doi:10.1126/science.1234204
582　Bujak, J. P., & Williams, G. L. (1977). Jurassic palynostratigraphy of offshore eastern Canada. In
583　　　　F. M. Swain (Ed.), *Stratigraphic Micropaleontology of Atlantic Basin and Borderlands,*
584　　　　*Developments in Paleontology and Stratigraphy* (Vol. 6, pp. 321-339). Amsterdam:
585　　　　Elsevier.
586　Callot, J. P., Ribes, C., Kergaravat, C., Bonnel, C., Temiz, H., Poisson, A., Vrielynck, B., Salel, J. F.,
587　　　　& Ringenbach, J. C. (2014). Salt tectonics in the Sivas basin (Turkey): crossing salt walls
588　　　　and minibasins. *Bulletin De La Societe Geologique De France, 185*(1), 33-42. doi:DOI
589　　　　10.2113/gssgfbull.185.1.33
590　Cirilli, S., Marzoli, A., Tanner, L., Bertrand, H., Buratti, N., Jourdan, F., Bellieni, G., Kontak, D., &
591　　　　Renne, P. R. (2009). Latest Triassic onset of the Central Atlantic Magmatic Province
592　　　　(CAMP) volcanism in the Fundy Basin (Nova Scotia): New stratigraphic constraints. *Earth*
593　　　　*and Planetary Science Letters, 286*(3-4), 514-525. doi:10.1016/j.epsl.2009.07.021
594　Davies, J., Marzoli, A., Bertrand, H., Youbi, N., Ernesto, M., & Schaltegger, U. (2017). End-Triassic
595　　　　mass extinction started by intrusive CAMP activity. *Nat Commun, 8*, 15596.
596　　　　doi:10.1038/ncomms15596
597　Densmore, A. L., Dawers, N. H., Gupta, S., Guidon, R., & Goldin, T. (2004). Footwall topographic
598　　　　development during continental extension. *Journal of Geophysical Research-Earth*
599　　　　*Surface, 109*(F3). doi:10.1029/2003jf000115
600　Deptuck, M. E., & Altheim, B. (2018). Rift basins of the central LaHave Platform, offshore Nova
601　　　　Scotia. *CNSOPB Geoscience Open File Report, 2018-001MF*, 1-34.
602　Diegel, F. A., Karlo, J. F., Schuster, D. C., Shoup, R. C., & Tauvers, P. R. (1995). Cenozoic structural
603　　　　evolution and tectono-stratigraphic framework of the northern Gulf coast continental
604　　　　margin. In M. P. A. Jackson, D. G. Roberts, & S. Snelson (Eds.), *Salt tectonics: a global*
605　　　　*perspective* (Vol. 65, pp. 109-1051): AAPG Memoir.
606　Dostal, J., & Durning, M. (1998). Geochemical constraints on the origin and evolution of early
607　　　　Mesozoic dikes in Atlantic Canada. *European Journal of Mineralogy, 10*, 79-93.
608　Dostal, J., & Greenough, J. D. (1992). Geochemistry and petrogenesis of the early Mesozoic
609　　　　North Mountain Basalts of Nova Scotia, Canada. In J. H. Puffer & P. C. Ragland (Eds.),
610　　　　*Eastern North American Mesozoic Magmatism* (Vol. 268): Geological Society of America,
611　　　　Special Paper.
612　Dunn, A. M., Reynolds, P. H., Clarke, D. B., & Ugidos, J. M. (1998). A comparison of the age and
613　　　　composition of the Shelburne dyke, Nova Scotia, and the Messejana dyke, Spain.
614　　　　*Canadian Journal of Earth Sciences, 35*(10), 1110-1115.

615   Elliott, G. M., Wilson, P., Jackson, C. A.-L., Gawthorpe, R. L., Michelsen, L., & Sharp, I. R. (2012).
616   The linkage between fault throw and footwall scarp erosion patterns: An example from
617   the Bremstein Fault Complex, offshore Mid-Norway. *Basin Research, 24*, 180-197.
618   doi:10.1111/j.1365-2117.2011.00524.
619   Ford, M., Rohais, S., Williams, E. A., Bourlange, S., Jousselin, D., Backert, N., & Malartre, F.
620   (2013). Tectono-sedimentary evolution of the western Corinth rift (Central Greece).
621   *Basin Research, 25*(1), 3-25. doi:10.1111/j.1365-2117.2012.00550.x
622   Gawthorpe, R. L., Hurst, J. M., & Sladen, C. P. (1990). Evolution of Miocene footwall-derived
623   coarse-grained deltas, Gulf of Suez, Egypt: Implications for Exploration. *AAPG Bulletin,*
624   *74*(7), 1077-1086.
625   Gawthorpe, R. L., & Leeder, M. R. (2000). Tecton-sedimentary evolution of active extensional
626   basins. *Basin Research, 12*, 195-2018.
627   Ge, H., Jackson, M. P. A., Vendeville, B. C., Maier, M. O., & Handschy, J. W. (1997a).
628   Deformation of Prograding Wedges over a Ductile Layer—Applications of Physical
629   Models to Geologic Examples. *Gulf Coast Association of Geological Societies*
630   *Transactions, XLVII*, 177-184.
631   Ge, H. X., Jackson, M. P. A., & Vendeville, B. C. (1997b). Kinematics and dynamics of salt
632   tectonics driven by progradation. *AAPG Bulletin, 81*(3), 398-423.
633   Gibling, M. R., Culshaw, N., Rygel, M. C., & Pascucci, V. (2008). The Maritimes Basin of Atlantic
634   Canada: Basin Creation and Destruction in the Collisional Zone of Pangea. In
635   *Sedimentary Basins of the World* (Vol. 5, pp. 211-244).
636   Goteti, R., Ings, S. J., & Beaumont, C. (2012). Development of salt minibasins initiated by
637   sedimentary topographic relief. *Earth and Planetary Science Letters, 339-340*, 103-116.
638   doi:10.1016/j.epsl.2012.04.045
639   Gupta, S., Underhill, J. R., Sharp, I. R., & Gawthorpe, R. L. (1999). Role of fault interactions in
640   controlling synrift sediment dispersal patterns: Miocene, Abu Alaqa Group, Suez Rift,
641   Sinai, Egypt. *Basin Research, 11*(2), 167-189.
642   Hafid, M. (2000). Triassic-early Liassic extensional systems and their Tertiary inversion,
643   Essaouira Basin (Morocco). *Marine and Petroleum Geology, 17*, 409 - 429.
644   Hafid, M., Zizi, M., Bally, A. W., & Ait Salem, A. (2006). Structural styles of the western onshore
645   and offshore termination of the High Atlas, Morocco. *Comptes Rendus Geoscience,*
646   *338*(1-2), 50-64. doi:10.1016/j.crte.2005.10.007
647   Holser, W. T., Clement, G. P., Jansa, L. F., & Wade, J. A. (1988). Evaporite deposits of the North
648   Atlantic rift. *Development in Geotectonics, 22*, 525-556.
649   Hopkins, M. C., & Dawers, N. H. (2018). The role of fault length, overlap and spacing in
650   controlling extensional relay ramp fluvial system geometry. *Basin Research, 30*(1), 20-
651   34. doi:10.1111/bre.12240
652   Hudec, M. R., & Jackson, M. P. A. (2011). *The salt mine: A digital atlas of salt tectonics*.
653   Hudec, M. R., Jackson, M. P. A., & Schultz-Ela, D. D. (2006). The paradox of minibasin
654   subsidence into salt: Clues to the evolution of crustal basins. *Geological Society of*
655   *America Bulletin, preprint*(2008). doi:10.1130/b26275.1
656   Jackson, C. A. L., Jackson, M. P. A., Hudec, M. R., & Rodriguez, C. R. (2015). Enigmatic structures
657   within salt walls of the Santos Basin—Part 1: Geometry and kinematics from 3D seismic

658   reflection and well data. *Journal of Structural Geology, 75*, 135-162.
659   doi:10.1016/j.jsg.2015.01.010

660 Jansa, L. F., Bujak, J. P., & Williams, G. L. (1980). Upper Triassic salt deposits of the western
661   North Atlantic. *Canadian Journal of Earth Sciences, 17*(5), 547-559.

662 Jourdan, F., Marzoli, A., Bertrand, H., Cirilli, S., Tanner, L. H., Kontak, D. J., McHone, G., Renne,
663   P. R., & Bellieni, G. (2009). 40Ar/39Ar ages of CAMP in North America: Implications for
664   the Triassic–Jurassic boundary and the 40K decay constant bias. *Lithos, 110*(1-4), 167-
665   180. doi:10.1016/j.lithos.2008.12.011

666 Leeder, M. R., & Jackson, J. A. (1993). The interaction between normal faulting and drainage in
667   active extensional basins, with examples from the western United States and central
668   Greece. *Basin Research, 5*, 79-102.

669 MacLean, B. C., & Wade, J. A. (1992). Petroleum Geology of the Continental-Margin South of
670   the Islands of St-Pierre and Miquelon, Offshore Eastern Canada. *Bulletin of Canadian
671   Petroleum Geology, 40*(3), 222-253.

672 MacLean, B. C., & Wade, J. A. (1993). East Coast Basin Atlas Series: Seismic markers and
673   stratigraphic picks in the Scotian Basin wells. *Geological Survey of Canada*, 276.

674 Manspeizer, W. (1988). A Stratigraphic Record from Morocco and North-America of Rifting,
675   Drifting and Tethyan Transgressions of the Central Proto-Atlantic. *Journal of African
676   Earth Sciences, 7*(2), 369-373. doi:Doi 10.1016/0899-5362(88)90081-4

677 Manspeizer, W., & Cousminer, H. L. (1988). Late Triassic-Early Jurassic synrift basins of the U.S.
678   Atlantic margin. In R. E. Sheridan & J. A. Grow (Eds.), *The Geology of North America, The
679   Atlantic Continental Margin* (Vol. I-2, pp. 197-216): Geological Society of America.

680 Martin-Martin, J. D., Verges, J., Saura, E., Moragas, M., Messager, G., Baques, V., Razin, P.,
681   Grelaud, C., Malaval, M., Joussiaume, R., Casciello, E., Cruz-Orosa, I., & Hunt, D. W.
682   (2017). Diapiric growth within an Early Jurassic rift basin: The Tazoult salt wall (central
683   High Atlas, Morocco). *Tectonics, 36*(1), 2-32. doi:10.1002/2016tc004300

684 Marzoli, A., Bertrand, H., Youbi, N., Callegaro, S., Merle, R., Reisberg, L., Chiaradia, M.,
685   Brownlee, S. I., Jourdan, F., Zanetti, A., Davies, J. H. F. L., Cuppone, T., Mahmoudi, A.,
686   Medina, F., Renne, P. R., Bellieni, G., Crivellari, S., El Hachimi, H., Bensalah, M. K.,
687   Meyzen, C. M., & Tegner, C. (2019). The Central Atlantic Magmatic Province (CAMP) in
688   Morocco. *Journal of Petrology, 60*(5), 945-996. doi:10.1093/petrology/egz021

689 Marzoli, A., Callegaro, S., Dal Corso, J., Davies, J. H. F. L., Chiaradia, M., Youbi, N., Bertrand, H.,
690   Reisberg, L., Merle, R., & Jourdan, F. (2018). The Central Atlantic Magmatic Province
691   (CAMP): A Review. In *The Late Triassic World* (pp. 91-125).

692 Marzoli, A., Jourdan, F., Puffer, J. H., Cuppone, T., Tanner, L. H., Weems, R. E., Bertrand, H.,
693   Cirilli, S., Bellieni, G., & De Min, A. (2011). Timing and duration of the Central Atlantic
694   magmatic province in the Newark and Culpeper basins, eastern U.S.A. *Lithos, 122*(3-4),
695   175-188. doi:10.1016/j.lithos.2010.12.013

696 McHone, J. G. (1992). Mafic dike suites within Mesozoic igneous provinces of New England and
697   Atlantic Canada. *Geological Society of America Special Paper, 268*.

698 Medina, F. (1995). Syn- and postrift evolution of the El Jadida - Agadir basin (Morocco):
699   constraints for the rifting model of the central Atlantic. *Canadian Journal of Earth
700   Sciences, 32*, 1273 - 1291.

701   OETR. (2014). *Offshore Energy Technical Research Association. Play Fairway Analysis -*
702   *Laurentian Basin, Canada. Nova Scotia Department of Energy.* Retrieved from
703   https://energy.novascotia.ca/oil-and-gas/offshore/play-fairway-
704   analysis/analysis/laurentian-sub-basin
705   Olsen, P. E. (1997). Stratigraphic record of the early Mesozoic breakup of Pangea in the
706   Laurasia-Gondwana rift system. *Annual Review of Earth and Planetary Sciences, 25*, 337-
707   401. doi:10.1146/annurev.earth.25.1.337
708   Olsen, P. E., & Et-Touhami, M. (Eds.). (2008). *Field trip 1: Tropic to subtropical syntectonic*
709   *sedimentation in the Permian to Jurassic Fundy rift basin, Atlantic Canada, in relation to*
710   *the Moroccan conjugate margin*. Halifax, N. S., Canada: Dalhousie University.
711   Olsen, P. E., Kent, D. V., Cornet, B., Witte, W. K., & Schlische, R. W. (1996). High-resolution
712   stratigraphy of the Newark rift basin (early Mesozoic, eastern North America).
713   *Geological Society of America Bulletin, 108*(1), 40-77. doi:10.1130/0016-
714   7606(1996)108<0040:Hrsotn>2.3.Co;2
715   Olsen, P. E., Kent, D. V., Et-Touhami, M., & Puffer, J. (2003). Cyclo-, magneto-, and bio-
716   stratigraphic constraints on the duration of the CAMP event and its relationship to the
717   Triassic-Jurassic boundary. *The Central Atlantic magmatic province: insights from*
718   *fragments of Pangea*, 7-32.
719   Olsen, P. E., & Schlische, R. W. (1990). Transtensional Arm of the Early Mesozoic Fundy Rift
720   Basin - Penecontemporaneous Faulting and Sedimentation. *Geology, 18*(8), 695-698.
721   doi:Doi 10.1130/0091-7613(1990)018<0695:Taotem>2.3.Co;2
722   Pe-Piper, G., Jansa, L. F., & Lambert, R. (1992). Early Mesozoic magmatism on the eastern
723   Canadian margin: petrogenetic and tectonic significance. *Geological Society of America*
724   *Special Paper, 268*, 13-36.
725   Peacock, D. C. P., & Sanderson, D. J. (1991). Displacements, segment linkage and relay ramps in
726   normal fault zone. *Journal of Structural Geology, 16*(6), 721-733.
727   Planke, S., Alvestad, E., & Eldholm, O. (1999). Seismic characteristics of basaltic extrusive and
728   intrusive rocks. *The Leading Edge, 18*(3), 342-348. doi:10.1190/1.1438289
729   Planke, S., Rasmussen, T., Rey, S. S., & Myklebust, R. (2005). *Seismic characteristics and*
730   *distribution of volcanic intrusions and hydrothermal vent complexes in the Vøring and*
731   *Møre basins.* Paper presented at the Geological Society, London, Petroleum Geology
732   Conference series.
733   Rowan, M. G. (2019). Conundrums in loading-driven salt movement. *Journal of Structural*
734   *Geology, 125*, 256-261. doi:10.1016/j.jsg.2018.04.010
735   Rowan, M. G., Peel, F. J., & Vendeville, B. C. (2004). Gravity-driven Fold Belts on Passive
736   Margins. In K. R. McClay (Ed.), *Thrust tectonics and hydrocarbon systems* (pp. 157-182).
737   Rowan, M. G., Urai, J. L., Fiduk, J. C., & Kukla, P. A. (2019). Deformation of intrasalt competent
738   layers in different modes of salt tectonics. *Solid Earth, 10*(3), 987-1013. doi:10.5194/se-
739   10-987-2019
740   Saura, E., Verges, J., Martin-Martin, J. D., Mesager, G., Moragas, M., Razin, P., Grelaud, C.,
741   Joussiaume, R., Malaval, M., Homke, S., & Hunt, D. W. (2014). Syn- to post-rift diapirism
742   and minibasins of the Central High Atlas (Morocco): the changing face of a mountain
743   belt. *Journal of the Geological Society, 171*(1), 97-105. doi:10.1144/jgs2013-079

744   Schlische, R. W., Withjack, M. O., & Eisenstadt, G. (2002). An experimental study of the
745   secondary deformation produced by oblique-slip normal faulting. *AAPG Bulletin, 86*(5),
746   885-906.
747   Schlische, R. W., Withjack, M. O., & Olsen, P. E. (2003). Relative Timing of CAMP, Rifting,
748   Continental Breakup, and Basin Inversion: Tectonic Significance. In W. E. Hames, J. G.
749   McHone, P. R. Renne, & C. Ruppel (Eds.), *The Central Atlantic Magmatic Province,*
750   *Insights from Fragments of Pangea* (Vol. 136, pp. 33-59): American Geophysical Union,
751   Geophysical Monograph.
752   Sinclair, I. K. (1993). Tectonism: the dominant factor in mid-Cretaceous deposition in the Jeanne
753   d'Arc Basin, Grand Banks. *Marine and Petroleum Geology, 10*, 530-549.
754   Sinclair, I. K. (1995). Transpressional inversion due to episodic rotation of extensional stresses in
755   Jeanne d'Arc Basin, offshore Newfoundland. In J. G. Buchanan & P. G. Buchanan (Eds.),
756   *Basin Inversion* (Vol. 88, pp. 249-271).
757   Sinclair, I. K., Evans, J. E., Albrechtsons, E. A., & Sydora, L. J. (1999). The Hibernia Oilfield -
758   effects of episodic tectonism on structural character and reservoir
759   compartmentalization. *Petroleum Geology of Northwest Europe: Proceedings of the 5th*
760   *Conference*, 517-528.
761   Sues, H.-D., & Olsen, P. E. (2015). Stratigraphic and temporal context and faunal diversity of
762   Permian-Jurassic continental tetrapod assemblages from the Fundy rift basin, eastern
763   Canada. *Atlantic Geology, 51*(1). doi:10.4138/atlgeol.2015.006
764   Tankard, A. J., Welsink, H. J., & Jenkins, W. A. M. (1989). Structural styles and stratigraphy of the
765   Jeanne d'Arc Basin, Grand Banks of Newfoundland. In *Extensional tectonics and*
766   *stratigraphy of the North Atlantic margins: AAPG Memoir*.
767   Tanner, L. H., & Brown, D. E. (1999). The Upper Triassic Chedabucto Formation: Guysborough
768   County, Nova Scotia: depositional and tectonic context. *Atlantic Geology, 35*, 129-138.
769   Tanner, L. H., & Brown, D. E. (2003). *Tectonostratigraphy of the Orpheus graben, Scotian basin,*
770   *offshore eastern Canada, and its relationship to the Fundy rift basin* (Vol. 2): Columbia
771   University Press.
772   Tanner, L. H., & Hubert, J. F. (1991). Basalt breccias and conglomerates in the lower Jurassic
773   McCoy Brook Formation, Fundy basin, Nova Scotia: Differentiation of talus and debris-
774   flow deposits. *Journal of Sedimentary Petrology, 61*, 15-27.
775   Tari, G., & Jabour, H. (2013). Salt tectonics along the Atlantic margin of Morocco. *Geological*
776   *Society, London, Special Publications, 369*(1), 337-353. doi:10.1144/sp369.23
777   Teixell, A., Barnolas, A., Rosales, I., & Arboleya, M.-L. (2017). Structural and facies architecture
778   of a diapir-related carbonate minibasin (lower and middle Jurassic, High Atlas,
779   Morocco). *Marine and Petroleum Geology, 81*, 334-360.
780   doi:10.1016/j.marpetgeo.2017.01.003
781   Van Gent, H., Urai, J. L., & de Keijzer, M. (2011). The internal geometry of salt structures – A
782   first look using 3D seismic data from the Zechstein of the Netherlands. *Journal of*
783   *Structural Geology, 33*(3), 292-311. doi:10.1016/j.jsg.2010.07.005
784   Verati, C., Rapaille, C., Féraud, G., Marzoli, A., Bertrand, H., & Youbi, N. (2007). 40Ar/39Ar ages
785   and duration of the Central Atlantic Magmatic Province volcanism in Morocco and
786   Portugal and its relation to the Triassic–Jurassic boundary. *Palaeogeography,*
787   *Palaeoclimatology, Palaeoecology, 244*(1-4), 308-325. doi:10.1016/j.palaeo.2006.06.033

788 Wade, J. A., & MacLean, B. C. (1990). The geology of of the southeastern margin of Canada. In
789   M. J. Keen & G. L. Williams (Eds.), *Geology of the continental margin of eastern Canada*
790   (pp. 167 - 238): Geological Survey of Canada, Geology of Canada.
791 Wade, J. A., MacLean, B. C., & Williams, G. L. (1995). Mesozoic and Cenozoic Stratigraphy,
792   Eastern Scotian Shelf - New Interpretations. *Canadian Journal of Earth Sciences, 32*(9),
793   1462-1473. doi:10.1139/e95-118
794 Welsink, H., & Tankard, A. (2012). Extensional tectonics and stratigraphy of the Mesozoic
795   Jeanne d'Arc basin, Grand Banks of Newfoundland. In A. W. Bally & D. G. Roberts (Eds.),
796   *Regional Geology and Tectonics: Phanerozoic Rift Systems and Sedimentary Basins* (pp.
797   373-381). Amsterdam: Elsevier.
798 Weston, J. F., MacRae, R. A., Ascoli, P., Cooper, M. K. E., Fensome, R. A., Shaw, D., & Williams,
799   G. L. (2012). A revised biostratigraphic and well-log sequence-stratigraphic framework
800   for the Scotian Margin, offshore eastern Canada. *Canadian Journal of Earth Sciences,*
801   *49*(12), 1417-1462. doi:10.1139/e2012-070
802 White, C. E., Kontak, D. J., DeMont, G. J., & Archibald, D. (2017). Remnants of Early Mesozoic
803   basalt of the Central Atlantic Magmatic Province in Cape Breton Island, Nova Scotia,
804   Canada. *Canadian Journal of Earth Sciences, 54*(4), 345-358. doi:10.1139/cjes-2016-0181
805 Withjack, M. O., Baum, M. S., & Schlische, R. W. (2010). Influence of preexisting fault fabric on
806   inversion-related deformation: A case study of the inverted Fundy rift basin,
807   southeastern Canada. *Tectonics, 29*(6), n/a-n/a. doi:10.1029/2010tc002744
808 Withjack, M. O., & Callaway, S. (2000). Active normal faulting beneath a salt layer: An
809   experimental study of deformation patterns in the cover sequence. *AAPG Bulletin, 84*(5),
810   627-651.
811 Withjack, M. O., & Schlische, R. W. (2005). *A Review of Tectonic Events on the Passive Margin of*
812   *Eastern North America*. Paper presented at the 25th Annual Bob F. Perkins Research
813   Conference, Houston, Texas.
814 Withjack, M. O., Schlische, R. W., & Baum, M. S. (2009). Extensional development of the Fundy
815   rift basin, southeastern Canada. *Geological Journal, 44*(6), 631-651. doi:10.1002/gj.1186
816 Withjack, M. O., Schlische, R. W., Malinconico, M. L., & Olsen, P. E. (2013). Rift-basin
817   development: lessons from the Triassic–Jurassic Newark Basin of eastern North
818   America. *Geological Society, London, Special Publications, 369*(1), 301-321.
819   doi:10.1144/sp369.13
820 Withjack, M. O., Schlische, R. W., & Olsen, P. E. (1998). Diachronous rifting, drifting, and
821   inversion on the passive margin of central eastern North America: An analog for other
822   passive margins. *AAPG Bulletin, 82*(5), 817-835.
823 Withjack, M. O., Schlische, R. W., & Olsen, P. E. (2002). Rift-basin structure and its influence on
824   sedimentary systems. *SEPM Special Publication, 73*, 57-81.
825 Withjack, M. O., Schlische, R. W., & Olsen, P. E. (2012). Development of the passive margin of
826   Eastern North America: Mesozoic rifting, igneous activity, and breakup. In *Regional*
827   *Geology and Tectonics: Phanerozoic Rift Systems and Sedimentary Basins* (pp. 300-335).
828 Yilmaz, O. (1987). *Seismic Data Processing*. Tulsa, Oklahoma: Society of Exploration
829   Geophysicists.